

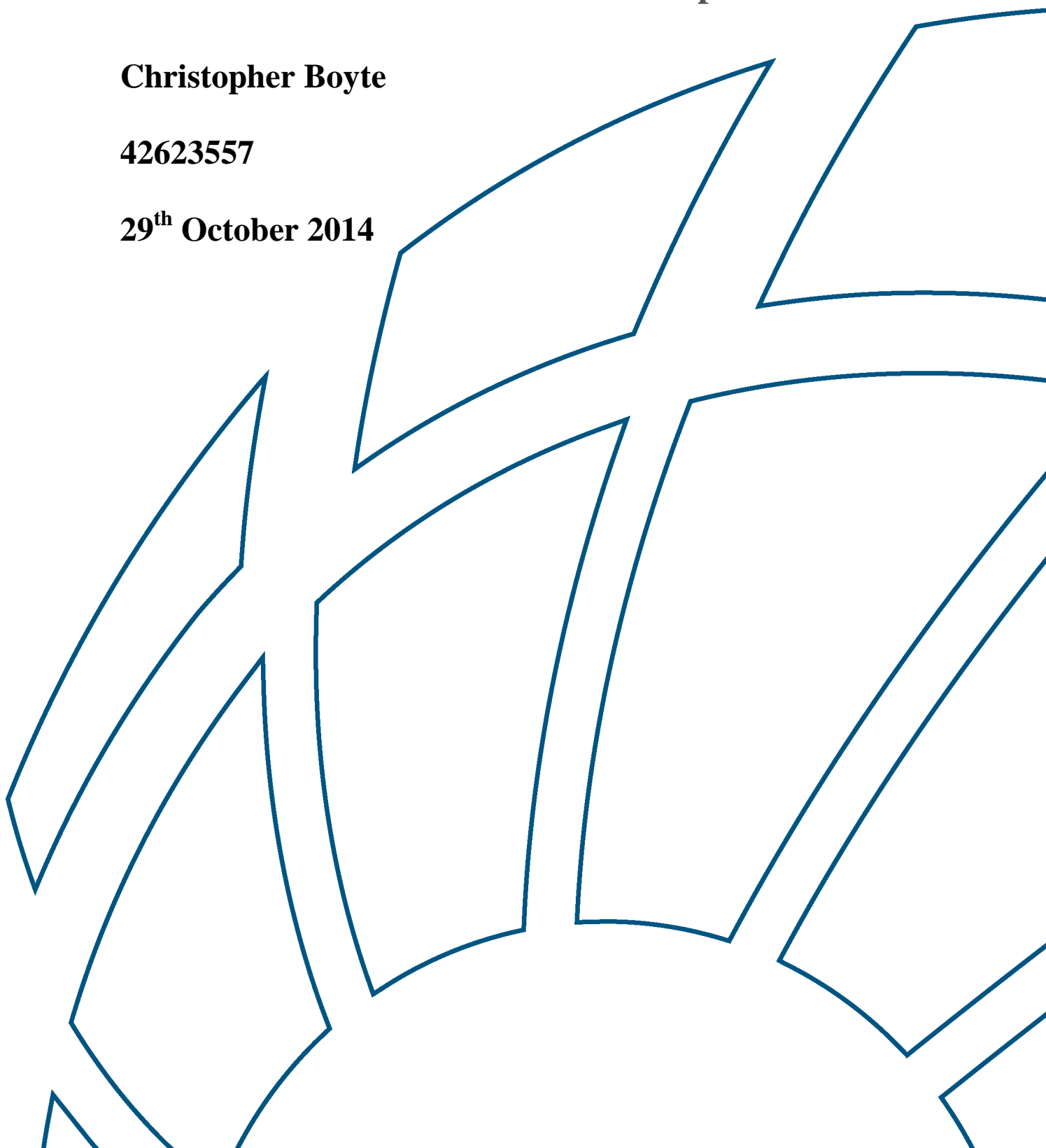


The Application of Direct Rainfall Models as Hydrologic Models Incorporating Hydraulic Resistance at Shallow Depths

Christopher Boyte

42623557

29th October 2014



29th October 2014

Professor Jose Torero

Head, School of Civil Engineering
St Lucia, QLD 4067

Christopher Boyte

2 Daniel Court

Scarborough, Queensland 4020

Dear Professor Torero,

I hereby submit my thesis titled "The Application of Direct rainfall models as Hydrologic Models Incorporating Hydraulic Resistance at Shallow Depth" for consideration as partial fulfilment of the Bachelor of Civil and Environmental Engineering degree.

All of the work contained within this thesis is my original work except where otherwise acknowledged.

I understand that this thesis may be made publicly available and reproduced by the University of Queensland unless a limited term embargo on publication has been negotiated with a sponsor.

Yours sincerely,

Christopher Michael Boyte

42623557

Acknowledgements

There are a number of people I would like to thank for their contributions to this study. Firstly, I am extremely grateful to my supervisor Dr David Callaghan, for the endless hours he spent giving insight and explanations for many concepts in this study.

To my industry supervisor, Bill Syme, I would like to thank for his time spent offering his insight to ensure the study was solving practical problems in dying need of solving at present, and also for his help with the explanation and adaptation of the TUFLOW source code.

I would also like to thank a number of work colleagues for their technical assistance on utilising the software packages present in the report - Michael Hughes, Rachel Jensen and Cecile Peille for their troubleshooting guidance on hydraulics and hydrologic modelling. I would also like to acknowledge thanks to Richard Sharpe for his data from his masters thesis, and thanks to the BMT WBM team as a whole for their support and the opportunity to use their fantastic software.

Finally, I would like to sincerely thank my loved ones; Tanya, Nick, and my parents, Andrew and Beverley Boyte - for their endless support and encouragement through what has been a challenging but valuable thesis in the final year of my undergraduate degree.

Abstract

This thesis is an investigation into incorporating hydrology into *direct rainfall models*, with consideration given to hydraulic resistance mechanisms at shallow flow. The direct rainfall methodology was implemented into a two dimensional shallow water model, TUFLOW GPU; which was compared against an industry standard hydrologic model, XP RAFTS.

The primary objectives were to determine whether TUFLOW GPU was a suitable software package to use in industry applications, whether the *direct rainfall model* was able to reproduce the hydrology of a real storm event in a gauged catchment more accurately than the hydrologic model; and to understand hydraulic resistance mechanisms at shallow flow and at different roughness scales. These objectives were met through numerical modelling with real data produced from experiments, stream gauges, or analytical solutions. Dressler's sloping dam break analytical model was used to validate TUFLOW GPU, a gauged catchment in New South Wales was used to compare hydrology representation in the *direct rainfall model* and hydrologic model, and experimental data from an open channel at shallow flow was analysed to analyse hydraulic resistance mechanisms. Monte Carlo testing by simulating non uniformity in bed roughness was undertaken on an ungauged catchment in New South Wales to determine the practical impacts of secondary flows, which arose after analysis of the experimental data.

Results of the model validation showed the shape and magnitude of the depth versus time curves produced from TUFLOW GPU matched Dressler's solution with high accuracy, indicating the shallow water model contains an effective Riemann solver and is capable of modelling discontinuity in mass and momentum flux. It was concluded the model was deemed fit for purpose and no further analysis was required. Results from the comparison between XP RAFTS (hydrologic software) and TUFLOW GPU (hydraulic software) on the gauged catchment in Durrumbul showed TUFLOW GPU reproduced the hydrology for a 2012 January storm event more accurately based on the timing and magnitudes of the peak and falling limb. Analysis of the experimental data showed mechanisms regarding hydraulic resistance to be related to the flow regime, which was dependent on the ratio of flow depth to roughness element height (termed relative submergence). A ratio less than one infers large scale roughness conditions, where bed shear, drag forces, form losses, and secondary flow are relevant for consideration in modelling the velocity distribution. A ratio greater than 4 infers small scale roughness conditions, where

only bed shear is relevant in the velocity distribution. A ratio within the range of 1 and 4 infers intermediate scale roughness conditions, which is an intermediary of the two roughness scale conditions. *The Law of the Wall* was found to be more suitable for modelling the velocity distribution at shallow flow when compared to *The Manning equation*, although secondary flows induced by the presence of non-uniformity in bed roughness created significant scatter in the experimental data used in the analysis. Neither method was able to correctly model flow at large scale roughness conditions. Results of the Monte Carlo test showed the variance in flow rate as a result of non-uniformity in bed roughness was negligible if the model was required for hydrology, but significant if an intricate study was being investigated, such as quantifying insurance claims for house inundation on an urban catchment.

The investigations of this thesis were limited by constraints of time and lack of experimental data, such that only rudimentary analyses could be performed. Based on these limitations and others, recommendations have been made for further studies be conducted for hydraulic resistance at shallow flow. In particular, it is highly recommended a comprehensive study on drag coefficients is conducted for emergent large scale roughness conditions, with recommendations given on modelling the velocity distribution. This stems from the inability of *The Law of the Wall* to predict the distribution, given its origin as a bed shear equation. Given the limited amount of data for shallow flow in open channels, the next step in this research would be to verify these conclusions align with independent experimental shallow flow data.

Table of Contents

Abstract	4
Table of Figures	8
Table of Tables.....	10
Notation.....	11
Terminology.....	12
1 Introduction.....	13
2 TUFLOW GPU Overview and Validation.....	19
2.1 TUFLOW GPU Overview	19
2.1.1 Numerical Scheme of TUFLOW GPU	19
2.1.2 Model Run Parallelisation.....	20
2.2 Model Validation.....	21
2.2.1 Procedure.....	22
2.2.2 Results and Discussion.....	23
2.3 TUFLOW GPU/CPU Sensitivity Testing	25
2.3.1 Procedure.....	25
2.3.2 Results and Discussion.....	26
3 Direct Rainfall Modelling Versus Hydrologic Models	27
3.1 Introduction	27
3.2 Hydrologic Model Benchmarking.....	27
3.3 Review of Hydrologic Models Commonly Used in Australia	28
3.4 Motivation for Change in the Hydrologic Model Approach.....	29
3.5 Direct rainfall modelling	31
3.5.1 Effect of Grid Size.....	32
3.5.2 Procedure - Comparison of Direct Rainfall Models and Hydrologic Models	33
3.5.3 Results and Discussion.....	35
4 Shallow Flow Hydraulics	38

4.1	Mechanisms of Flow Resistance	39
4.2	The History of the Development of Velocity Distribution.....	39
4.3	Studies Undertaken on Manning's n.....	40
4.4	Procedure for Large Scale Roughness Testing.....	48
4.4.1	Results and Discussion.....	50
4.5	The Law of the Wall (Logarithmic Velocity Law)	51
4.6	Comparison of Methods	55
4.6.1	Procedure.....	55
4.6.2	Results	56
4.7	Law of the Wall Implementation Into Numerical Model	59
4.8	Practical Implications of Secondary Flows	60
4.8.1	Introduction	60
4.8.2	Procedure.....	61
4.8.3	Results and Discussion.....	63
5	Conclusion and Further Research Directions	65
6	References	68
	Appendix 1 - Dressler Dam Break	72
	Appendix 2 - Pearson Correlation for Dressler's Dam Break Solution	73
	Appendix 3 - Sensitivity Testing of TUFLOW GPU.....	74
	Appendix 4 - TUFLOW GPU versus RAFTS on Gauged Catchment.....	75
	Appendix 5 - Roughness Calculation using the Root Mean Square of Surface Roughness	76
	Appendix 6 - TUFLOW Model for Large Scale Roughness Conditions (Emergent Reeds)	78
	Appendix 7 - Evidence of Data Collapse by Adjustment of z_0 parameter on the Log Law	79
	Appendix 8 - Data Summary of Jordanova	80
	Appendix 9 - Source Code of the Log Law implementation into TUFLOW (in FORTRAN)	81
	Appendix 10 - Practical Implications of Secondary Flows	82

Table of Figures

Figure 1 – Normalised velocity versus depth to roughness height ratio for the Manning's equation and the Log Law with experimental data, with specification of direct rainfall modelling and ocean modelling regions.	17
Figure 2 – Longitudinal section of Dressler's solution showing the wedge of water at time zero and Cartesian coordinates set-up using the wedge face at bed level as the origin (Dressler 1958)	22
Figure 3a - Propagation of the water wedge down the slope in the reference frame of the bed slope (i.e. the x axis corresponds to the bed). Each curve represents a different point in dimensionless time as shown in the legend, and where each axis represents a dimensionless length, with y corresponding to average depth, and x corresponding to longitudinal distance down the slope. The wedge is able to deform as the gate is collapsed at $T = 0$	23
Figure 4 - Spatial figure of a plan view of the channel in which the dam break occurs. The coloured contour corresponds to the wedge of water before the gate is released, and each dot in the channel corresponds to the static location at which the data is taken over time. These points correspond to the locations at which the curves in Figure 3b are taken.	24
Figure 5 - Dressler Validation of TUFLOW GPU of dimensionless depth versus dimensionless time. The results shown are constant spatially and taken as per Figure 2 with $Y = 1$. That is, -0.5 corresponds to the reference point of half of a wedge length back from the wedge front face (or the first dot in Figure 4), and 1 corresponds to the reference point of one wedge length in front of the wedge front face (or the second dot in Figure 4).	24
Figure 6 - Plan view of the numerical model set up. The dotted line corresponds to the model domain, and the grids correspond to the active cells in the model, which in this case is a single channel of cells, with a free overfall downstream boundary condition. Cell elevations were altered in order to achieve different slopes, and the water level was measured at the downstream end of the channel for comparison.	25
Figure 7 - Time of Concentration Vs. Manning's n, comparing the CPU and GPU solutions. A bed slope of 5%, 10%, and 15% was graphed, and Manning's n was varied from 0 (frictionless) up to 0.2 (extremely rough). The title of "GPU_5p" corresponds to a TUFLOW GPU run at 5% bed slope and so on.	26
Figure 8 - Comparison between different numerical methods for implementing a form of a hydrodynamic equation in accordance to Borah (2011).	28
Figure 9 – Relative model set-up comparison between RAFTS hydrologic model and TUFLOW GPU hydraulic model on gauged catchment in North Byron.	34
Figure 10 - TUFLOW GPU versus RAFTS for the real gauged catchment	35

Figure 11 - Relative accuracy of Manning's equation based against experimental data (Nikuradse 1950). Data is graphed using normalised mean velocity on the Y axis (which is normalised with the friction velocity) and relative submergence on the X axis.....41

Figure 12 - Comparison of Manning's n and F, graphed with stem density on the X axis and Manning's n/James' F on the Y axis. Manning's n plot on the left shows significant scatter with depth and James' F on the right shows a collapse in data points (Sharpe & James 2007).....46

Figure 13 - Numerical results for the 'Emergent Reeds' experiment using the 'Experimental Depth Measurement' as a downstream boundary condition.....50

Figure 14 – Example of the impact of element arrangement in large scale roughness conditions on the flow pattern.....50

Figure 15 - Concept of The Law of the Wall53

Figure 16 - Comparison of the Law of the Wall and the Manning Equation with the relationship between normalised velocity and relative roughness; showing all three relative roughness regions. Data was sourced from Jordanova (2008).....56

Figure 17 - Recreated velocity distribution over intermediate scale roughness, small scale roughness, and relative submergences which aren't suitable to model using a bed shear formula (i.e. ocean modelling). Data is graphed with normalised mean velocity on the Y axis, and relative submergence on the X axis. 'Nikuradse' and 'Moody' data was received from the original reports (Nikuradse 1950).....57

Figure 18 - Conceptual layout of the Law of the Wall for dimensional analysis. Mean velocity changes over the depth of the fluid and is dependent on bed shear, fluid density, and height within the fluid.58

Figure 19 - Bankstown catchment aerial showing relative land use and catchment boundary. The “PO” lines correspond to data collection points at which the flow rate is recorded with time. High elevation is recorded in red in the Digital elevation map and low elevation in blue.62

Figure 20 - Histograms of 'Plot Output' flow rates calculated with respect to variance in urban roughness. Frequency is shown on the vertical axis, and the relative variance in flow rate (m^3/s) is shown on the horizontal axis, which was calculated as a ratio of the flow range over the mean flow.63

Figure 21 - Semi Emperical Log-Law evidencing better correlation in the transition zone by using a curve fit for z_079

Table of Tables

Table 1 - Breakdown of the types of forces relevant in the Navier-Stokes equations with different relative depths of flow.....17

Table 2 – Summary of Figure 11, breaking up the *Calibration Gauge* curve into characteristics, and determining whether each numerical model accurately represents this characteristic in their results.36

Table 3 - Model conditions in TUFLOW for large scale roughness modelling.....49

Table 4 - A summary of equations which can be applied in the regions of the boundary layer where δ (m) is the boundary layer thickness and z (m) is the height above the solid boundary, and V_0 is the free stream velocity.....52

Table 5 - 95% confidence intervals for flow rate at each of the plot output lines shown in Figure 19.....63

Table 6 - Lack of Fit Assessment of TUFLOW GPU to Dressler's Solution.....73

Notation

Character	Description
S	Storage
I	Inflow
Q	Outflow/Flow Rate
k or K	Constant
u	Component of velocity in the x direction (cartesian system)
v	Component of velocity in the y direction (cartesian system)
w	Component of velocity in the z direction (cartesian system)
\bar{V}	Mean Velocity
u_f	Friction Velocity
d	Mean Hydraulic Depth
κ	Von Karmen Constant
k_s	Roughness Height
n	Manning's Coefficient
C	Chezy's Coefficient
A	Cross Section Area
\mathbb{F}	Froude Number
\mathbb{R}	Reynolds' Number
ρ	Density
z	Height above wall
g	Gravitational acceleration
t_c	Equilibrium time/time of concentration
ν	Dynamic Viscosity
τ	Shear Stress
S_0	Bed Slope
q	Discharge per unit width
f	Darcy Weisbach Friction Factor
C_{tot}	Form Loss Coefficient

m	Mass of object
F	Force
μ	Kinematic Viscosity
V	Velocity
T	Time
\bar{T}	Dimensionless Time
V_0	Free Stream Velocity
δ	Boundary Layer Thickness

Terminology

1D	One Dimensional
2D	Two Dimensional
3D	Three Dimensional
SWE	Shallow Water Equation
FDM	Finite Difference Method
FEM	Finite Element Method
FVM	Finite Volume Method
CPU	Central Processing Unit
GPU	Graphical Processing Unit
GIS	Geographic Information System
DEM	Digital Elevation Model

1 Introduction

Flood studies are useful tools to quantify the impacts of land changes and damages induced from storm events, amongst a multitude of other uses. The current industry standard is for flood models to utilise both hydrologic and hydraulic components. Hydrology first identifies the relevant catchments draining into the area of interest, then develops catchment parameters to hydrologically route storage to the boundary of the area of interest. Boundary flows are then utilised to hydraulically route through the area of interest in order to assess the flood extents and other behaviour.

The hydrology component is implemented through a hydrologic model, which exhibits two processes - converting rainfall to catchment runoff, and routing the runoff through the catchment. Hydrologic routing is based fundamentally on the storage equation,

$$\frac{\partial S}{\partial t} = I(t) - O(t) \quad (2.1)$$

where S (m^3) is the storage component, t (s) is time, I (m^3/s) is the inflow, and O (m^3/s) is the outflow. This is a simple lumped water balance, and is further developed into a simplified equation for overland flow containing a number of lumped catchment parameters, termed the Muskingum method (Carroll 1998). The application of hydrologic modelling software using these fundamental principles is predominant in the Australian market. However, these common approaches are limited due to the oversimplification of the physical process. Examples of this include the lumping of infiltration and interception stores, and the lumping of groundwater flow, interflow and direct runoff. This method also assumes the sub-catchments are well defined and no crossover will occur during significant events (Rehman et al. 2003). Although a higher level of accuracy may be achieved through model calibration, it is unlikely to correctly represent these physical processes simply by calibrating catchment parameters. The water balance approach is not momentum conservative which can also have adverse effects on model accuracy (Downer & Ogden 2004).

Hydraulic models have less modelling simplifications than hydrologic models, hence have more complexity and are more physically based. In order to gain an understanding of hydraulic models, the Navier-Stokes equations must first be understood. The equations arise from applying

Newton's second law to fluid motion, assuming the stress in the fluid is the summation of the viscous and pressure terms (Von Karman 1975). They are given in vector form by;

$$\overbrace{\rho\left(\frac{\partial V}{\partial t} + V.\Delta V\right)}^{ma} = \overbrace{-\Delta p + \mu(\Delta^2 V) + R}^{\Sigma F} \quad (2.2)$$

Inertia
Pressure
Viscosity
Boundary

Gradient

Conditions

where $V = \begin{bmatrix} u \\ v \\ w \end{bmatrix}$, and R is a boundary condition term capable of encompassing external forces

which are typically hydraulic resistance, Coriolis effects, wind stress etc.

Hydraulic models used in this study implement the two dimensional shallow water equations [SWEs], which are a relatively simplistic form of the Navier-Stokes equations. The two dimensional Shallow Water equations are derived by integrating the three dimensional Navier-Stokes equations along the depth of the fluid body, assuming uniform velocity profile, hydrostatic forces, incompressible fluid, and all source/sink terms of equation (2.2) can be applied as boundary conditions (Cunge 1980). Physically, the velocity profile is described by the boundary layer so the uniform velocity profile assumption is incorrect, though these discrepancies are typically accounted for in the source/sink term of equation (2.2). The SWEs are given the following equation to conserve the mass of the fluid (Toro 2009b);

$$\frac{\partial V}{\partial t} + \frac{\partial G}{\partial x} + \frac{\partial H}{\partial y} = 0. \quad (2.3)$$

Where vectors V, G, H can be expressed in terms of variables u, v, g, h as;

$$V = \begin{bmatrix} h \\ uh \\ vh \end{bmatrix}, G = \begin{bmatrix} uh \\ u^2h + \frac{gh^2}{2} \\ uvh \end{bmatrix}, H = \begin{bmatrix} vh \\ uvh \\ v^2h + \frac{gh^2}{2} \end{bmatrix}$$

where h is the water depth, g is the acceleration due to gravity and u and v are the flow velocities in the x and y direction.

These shallow water equations are used for hydraulic routing, in which recent advances in flood modelling methodology has brought focus to the *rain on grid* method; which works on the principle of applying an excess rainfall time-series directly to each active cell in the 2D model domain. Water accumulates in each cell to reach a specified depth, before propagating to adjacent cells based on the local slope and bed resistance through application of the shallow water equations.

Compared to the hydrologic methods, the *rain on grid* or *direct rainfall method* is significantly more detailed approach with especially beneficial uses for rural catchments with little available aerial photography, and catchments with insufficient topography change making it difficult to define flow paths. This is particularly useful for modelling complex situations which hydrologic methods tend to oversimplify (Borah 2011). However, the extra complexity comes with the cost of a computation time magnitudes slower than those of traditional hydrologic models; which arises largely from the number of cells needed in a hydraulic model compared to a hydrologic model (Kuo et al. 2011).

Previously, this necessitated a compromise between fast run times and model complexity, resulting in the use of hydrologic models due to economics. However, rapid advances in computing technology have led to the development of a significantly faster method to run models using Graphical Processing Units. NVIDIA have developed an algorithm capable of parallel computing - the Compute Unified Device Architecture (Anonymous 2009). The GPU framework is comprised of a number of functions, named kernels, which generate a large number of threads to exploit data parallelism. This approach utilises both Graphics Processing Units (GPU) and Central Processing Units (CPU) to speed up the implementation of the numerical solution, causing models to run up to 100 times faster.

Developed by WBM Pty Ltd., TUFLOW is a flood and tide simulation software package capable of accurately modelling the hydrodynamics for floodplains, rivers, estuaries and coastal waters. Since TUFLOW was first developed in 2001, it has progressed to accommodate for computation on both CPUs and GPUs (Syme 2006). The use of this industry accepted software reduces excessive run times with the parallel computation feature, such that it is now feasible to run a *direct rainfall model* in place of a paired hydrology/hydraulics model. However, the *direct*

rainfall model is a relatively new approach and as such, it contains components which have not been tested to gain a thorough conceptual understanding.

In light of this, hydraulic resistance at shallow flow is an area which has not been well researched. In *direct rainfall models*, a significant area of the model contains water flowing at very shallow depths which warrants the need for this research. The mean hydraulic depth and its relative scale to the size of the resisting elements in its flow path is a fundamental concept in understanding hydraulic resistance at shallow flow (Bathurst et al. 1981). In order to gain a brief understanding of how resistance changes at different scales, the following table was constructed.

Table 1 - Breakdown of the types of forces relevant in the Navier-Stokes equations with different relative depths of flow.



Sheet/Emergent Flow

- Runoff depth generally at a scale of millimetres (sometimes fractions of millimetres) to centimetres.
- Elements producing resistance are not completely submerged.
- Drag force, secondary flows and skin friction are very important in the velocity distribution.



Shallow Flow

- Runoff depth generally at a scale of centimetres.
- Elements producing resistance are submerged, but flow depth is still very shallow.
- Skin friction begins to dominate, but secondary flows and drag force are still significant in the velocity distribution.



Deep Flow

- Runoff depth at a scale of metres.
- Elements producing resistance are submerged, and flow is at least twice as deep as a shallow flow.
- Skin friction dominates in the velocity distribution.



Ocean Flow

- Runoff depth is orders of magnitude larger than a deep flow.
- Significant vertical velocities.
- Roughness terms are not significant in the hydrodynamic equations.
- Inertial terms dominate.

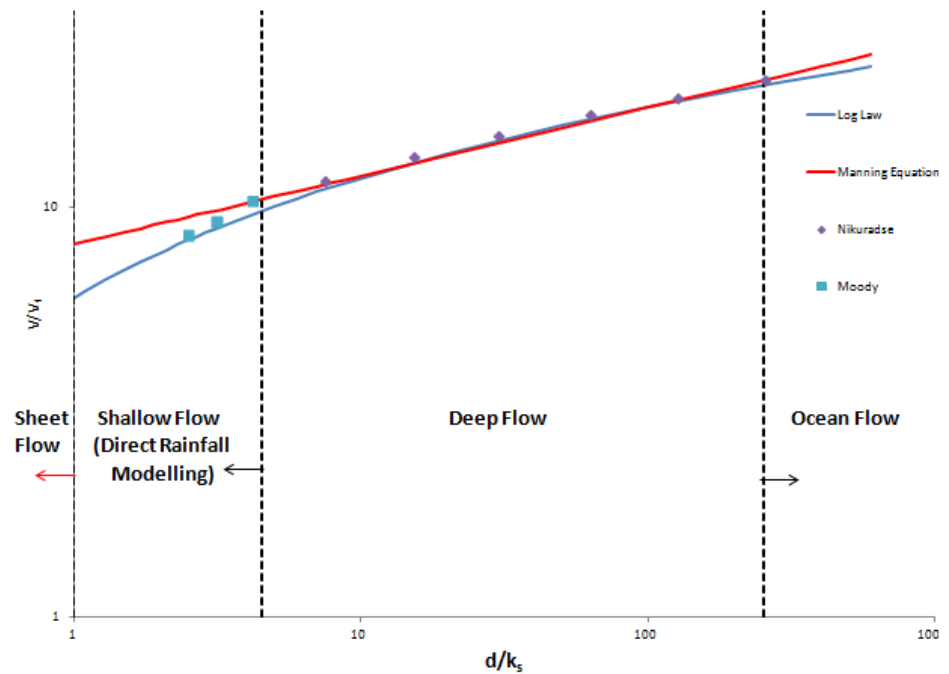


Figure 1 – Normalised velocity versus depth to roughness height ratio for the Manning's equation and the Log Law with experimental data, with specification of direct rainfall modelling and ocean modelling regions.

This report aims to validate and verify the application of direct rainfall hydraulic models for use in place of hydrologic models, with consideration given to hydraulic resistance at shallow depth. TUFLOW GPU will be primarily used as the software utilised for implementing a *direct rainfall model*.

A model validation will first be undertaken to determine the hydraulic model suitability. If the model is deemed suitable, it will be tested against commonly used hydrologic software in industry using an existing gauged catchment. Hydraulic resistance at shallow depth will be explored in great detail and data will be analysed using different methods for a comparison. Following comparison, the most appropriate method will be implemented and benchmarked in TUFLOW.

2 TUFLOW GPU Overview and Validation

2.1 TUFLOW GPU Overview

As with most models developed in the 1990's, TUFLOW Classic used a 2D implicit scheme with a finite difference solver. Previously this was the most economic choice due to the benefit of greater model stability at larger time steps – leading to faster and thus cheaper computation time. However, recent advances in technology have lead to parallel computation for explicit solvers. While parallel computation may be exploited for multiple Central Processing Unit (CPU) cores, Graphics Processing Units (GPUs) are generally opted for these modelling tasks due to the thousands of cores available per graphics card, which is in the range of two orders of magnitude greater number of cores than in a CPU, optimising computational efficiency.

For this reason, TUFLOW GPU was developed to create high resolution models with a more physical and potentially more accurate solution (due to its high resolution), solved up to two orders of magnitude faster compared to TUFLOW Classic's computation time.

2.1.1 Numerical Scheme of TUFLOW GPU

Discretisation method is an important choice for the numerical model scheme and will potentially influence the model accuracy and computational efficiency (LeVeque 2002). The use of finite element and finite difference methods can lead to spurious spatial oscillations due to nonlinear coupling between fluid depth and the horizontal velocity field resulting from the vertical integration of the 3D Navier-Stokes equations (Chippada et al. 1998). This is problematic as finite difference methods give spurious results for occurrences of discontinuities (such as hydraulic jumps and sharp bathymetry changes); while finite element methods are computationally inefficient due to the high number of mesh elements required to provide accurate solutions (Toro 2009a).

Hence, the discretisation method used in TUFLOW GPU is the finite volume method. This method provides an intermediary between the high accuracy of finite element method and the computationally efficient finite difference method (LeVeque 2002). The numerical model utilises Roe's method for solving the Riemann problem at the boundaries of the model cells. Roe's

method approximates a linear version of the Jacobian matrix and is then solved in accordance to Godunov's method. This has shown to be more computationally efficient and more suitable to use in hydraulic modelling (Toro 2009a). The finite volume discretisation method is utilised to implement the system of hydrodynamic nonlinear shallow water equations, in which the model assumes the assumptions of uniform velocity and Boussinesq theory hold true.

It is important to note that in practice, these assumptions are false. These assumptions neglect vertical frictional forces and non-hydrostatic forces which are actually present in real fluid flow. Callaghan et al. (2011) used a forced transient wave to prove the nonlinear shallow water equations show the best match with experimental data when non-hydrostatic and vertical frictional forces are included in the model. However, in absence of these non hydrostatic terms, a reasonable degree of accuracy is still able to be achieved in numerical models and due to the complexity of including these non-hydrostatic terms in the model, this will not be considered for this study.

2.1.2 Model Run Parallelisation

The primary difference between TUFLOW GPU and CPU models is the explicit finite volume scheme adopted in GPU, compared to the fully implicit finite difference scheme used for TUFLOW classic. FORTRAN CUDA is used as the programming language in TUFLOW GPU rather than FORTRAN, so that it may be adapted into the GPU framework created by NVIDIA. GPU functions, named kernels, generate a large number of threads to exploit data parallelism (Anonymous 2009). The model domain is divided into a set of computational blocks - to which threads are assigned to the blocks. Boundary conditions are assigned (with separate conditions on the domain boundary), and the SWEs are applied to computational blocks, with threads interacting within each block. The kernels update storage, solve continuity and momentum, and update boundary conditions; while the CPU adapt the timestep to ensure stability under the courant criterion (Kalyanapu et al. 2011; Toro 2009b). The solutions of TUFLOW GPU are first order spatial, but variable for the temporal scheme. Low order schemes are less memory intensive, but unstable with adaptive Runge Kutta [RK] methods - whereas high order temporal schemes are stable with adaptive RK methods (Collecot 2014).

In comparison to the existing hydrologic models, GPU models are substantially slower. This is largely due to the fact that for a given catchment, a TUFLOW GPU model may contain one

million elements within the FV grid; whereas an existing hydrologic model may only contain one hundred sub-catchments. This leads to a trade off between model complexity and computation time, where TUFLOW GPU aims to achieve a higher degree of accuracy in complex catchments compared to hydrologic models.

2.2 Model Validation

Model validation is a fundamental step in the modelling process to ensure the prediction model is able to correctly emulate necessary conditions formulated in the conceptual model. In this case, TUFLOW GPU must display sensible physics under difficult conditions to ensure the model is displaying the correct behaviour.

In this study, it was more desirable to use an analytical solution as the validation rather than an experiment; largely due to the possibility of measurement error in experiments. However, analytical solutions for the shallow water equations exist albeit with some assumptions which are generally non-applicable in practice. However, it is easier to create difficult situations in hydraulics in which a numerical model would struggle to reproduce, while the analytical solution maintains full control. A useful analytical solution of unsteady non-linear waves was derived by Dressler (1958), which was solved by neglecting hydraulic resistance in a sloping dam break scenario. The nature of the test is analogous to the steep catchments experienced when reproducing hydrology, which also makes this test practically suitable for this study, as well as technically challenging to match.

TUFLOW GPU was validated in this study using Dressler's solution, using a one dimensional triangular wedge of water as the initial condition. This validation is considered to be the most difficult test to emulate results with a numerical model due to the inherent modelling issues inherent within discretisation and scheme. An extremely steep slope, combined with a 2 dry fronts (dry cells in front and behind the moving water body) result in fluxes which approach infinity - making it difficult for most numerical models to solve. Dressler's solution also involves solving inverses of singular matrices, which makes it hard for most models to replicate the solution due to the mathematical challenge as well as the numerical challenge.

In addition to the above issues most models will have trouble overcoming, the solution is exact, which eliminates the experimental error associated with benchmarking using experimental data.

2.2.1 Procedure

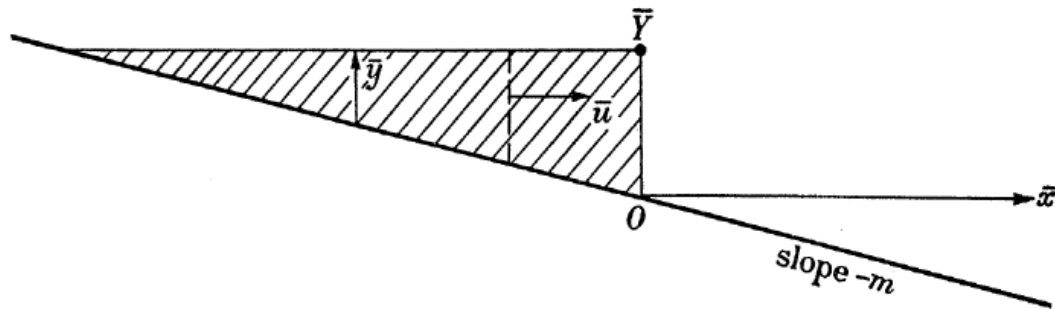


Figure 2 – Longitudinal section of Dressler’s solution showing the wedge of water at time zero and Cartesian coordinates set-up using the wedge face at bed level as the origin (Dressler 1958)

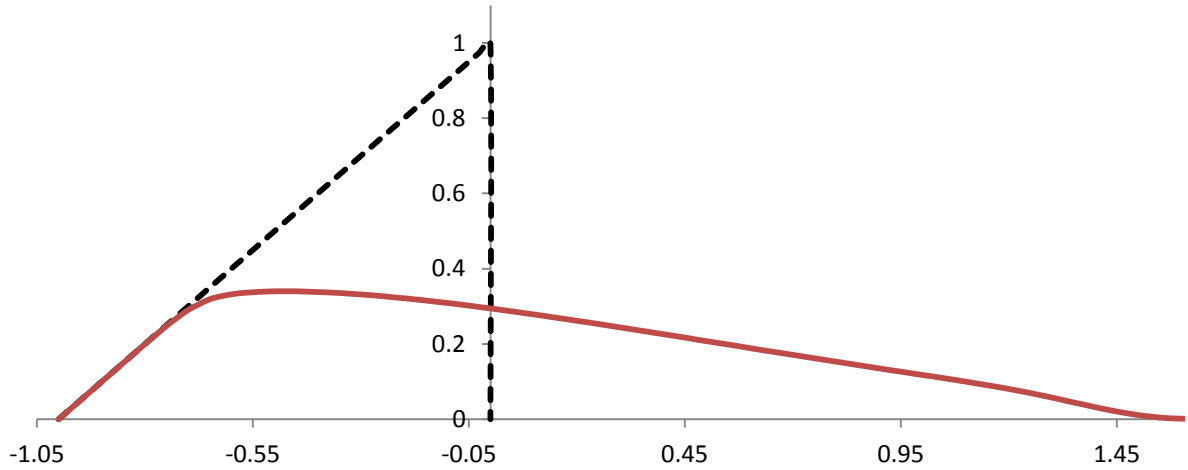
The analytical solution was derived taking a datum at the 0 point shown in Figure 2. Length and time scale are dimensionless where each dimension is converted on their relevant axis, i.e. longitudinal distance is made dimensionless by the division of the wedge length and so forth.

Time was made dimensionless through $\bar{T} = mT\sqrt{\frac{g}{Y}}$, where g is gravity, Y is wedge height, T is dimensional time, and m is the bed slope.

To replicate these conditions, a TUFLOW model was set up in MapInfo Professional (Anonymous 2014) with a grid size of 0.05m, and a channel composition of 20m by 0.4m. Plot Output points were placed at -0.5, 0.5, 1, and 2 dimensionless lengths along the channel and the depth and velocity were extracted at these points, before making them dimensionless and comparing to the Dressler solution. Dressler's solution was calculated using a Matlab script (Anonymous 2013) (Callaghan, Pers. Comm., 2014). All relevant files of the TUFLOW GPU set up and Dressler analytical solution can be found in Appendix 1.

2.2.2 Results and Discussion

a)



b)

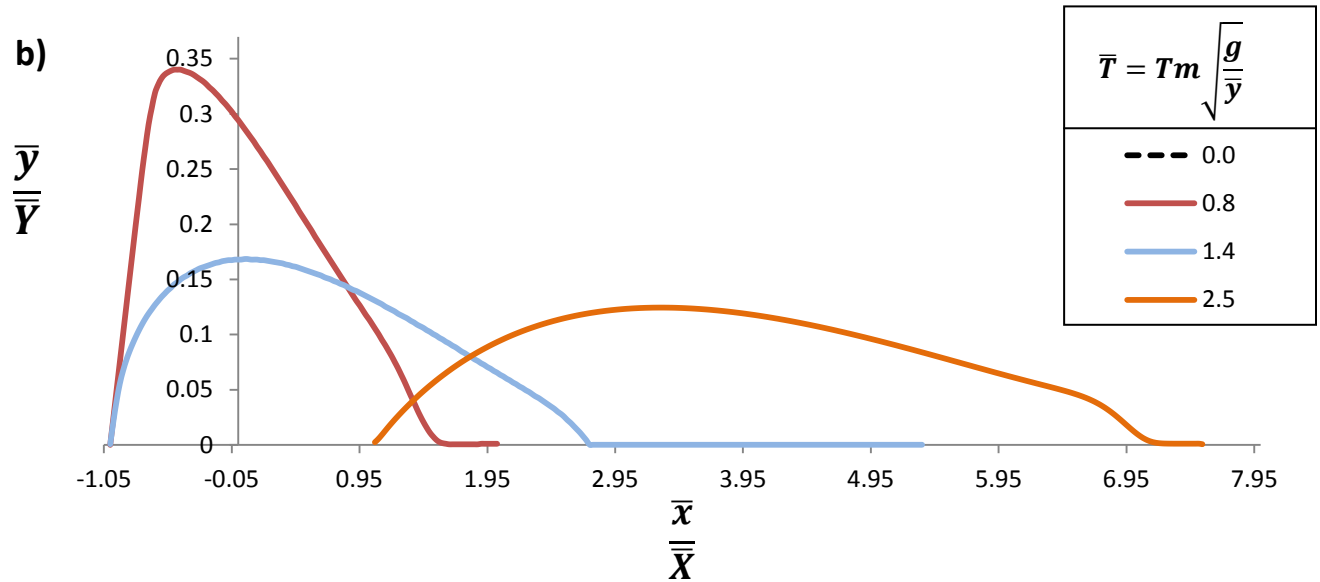


Figure 3a - Propagation of the water wedge down the slope in the reference frame of the bed slope (i.e. the x axis corresponds to the bed). Each curve represents a different point in dimensionless time as shown in the legend, and where each axis represents a dimensionless length, with \bar{y} corresponding to average depth, and \bar{x} corresponding to longitudinal distance down the slope. The wedge is able to deform as the gate is collapsed at $\bar{T} = 0$.

Figure 3b- The same figure as depicted in Figure 3a, but taken with different axes to show better representation of the deformation.



Figure 4 - Spatial figure of a plan view of the channel in which the dam break occurs. The coloured contour corresponds to the wedge of water before the gate is released, and each dot in the channel corresponds to the static location at which the data is taken over time. These points correspond to the locations at which the curves in Figure 3b are taken.

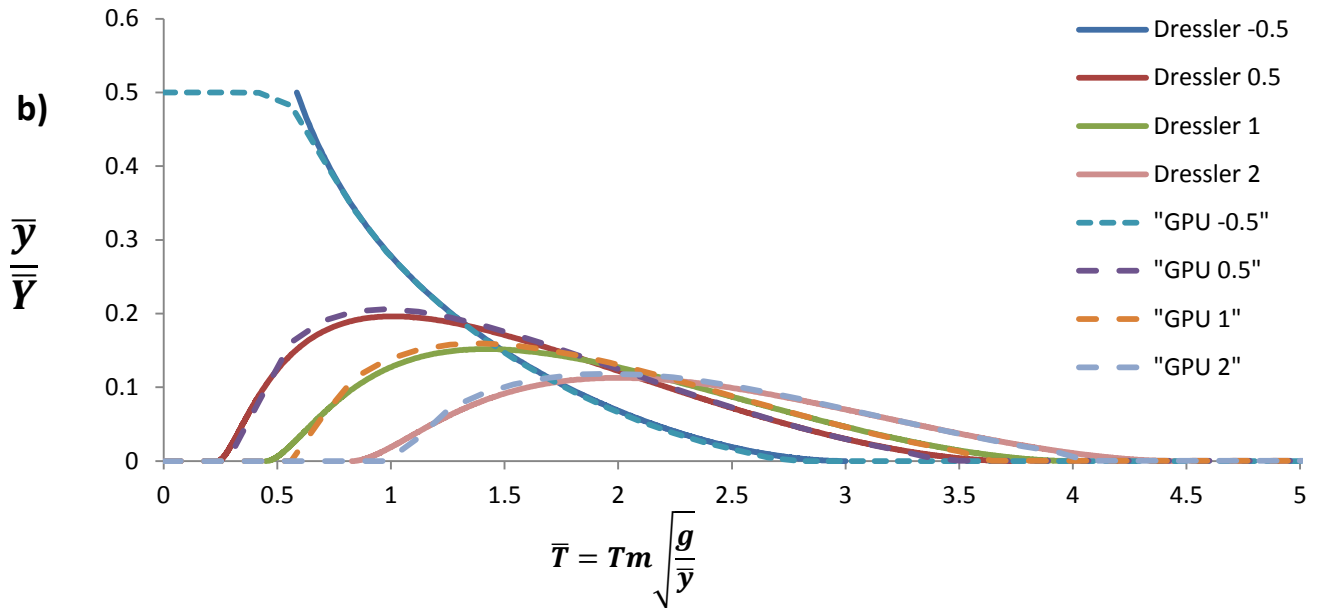


Figure 5 - Dressler Validation of TUFLOW GPU of dimensionless depth versus dimensionless time. The results shown are constant spatially and taken as per Figure 2 with $\bar{Y} = 1$. That is, -0.5 corresponds to the reference point of half of a wedge length back from the wedge front face (or the first dot in Figure 4), and 1 corresponds to the reference point of one wedge length in front of the wedge front face (or the second dot in Figure 4).

By visual inspection, it is obvious the timing and magnitude are slightly inaccurate in reproducing the analytical solution, but for the purposes of the numerical models use, it is considered to be an excellent fit - especially considering the nature of the test. The most important thing to note is the shape of the curves produced by the numerical software are suitable in comparison to the analytical solution. This result infers the numerical model correctly captures the physics modeled by Dressler's solution. No instability is evident from the wetting of dry cells and drying of wet cells as the advancing and trailing dry fronts are captured correctly. The implementation of the 2D shallow water equations on the GPU kernels (instead of onto each 2D grid cell) evidently doesn't sacrifice any accuracy on the correct physics of unsteady linear waves, as solved using Dressler's solution.

Pearson's correlation was undertaken to quantify the fit after it was determined to follow the correct shape by engineering judgment. The quantified results also showed a good fit ($R^2=0.999$). Results can be found in Appendix 2.

Considering the good fit of TUFLOW GPU to the analytical solution and the difficulty of the test, it is considered verified as an accurate model and hence is considered a reputable source to model outcomes for the rest of the study.

2.3 TUFLOW GPU/CPU Sensitivity Testing

Sensitivity Testing is an important part of model validation, and can be useful to test the significance of altering model parameters, as well as a useful comparison between two models. In this case, TUFLOW Classic and TUFLOW GPU will be compared using a sensitivity test of a one dimensional channel varying channel roughness and bed slope.

2.3.1 Procedure

MapInfo was used to set up a channel conveying one dimensional flow, with dimensions 1m by 100m as shown in Figure 6.

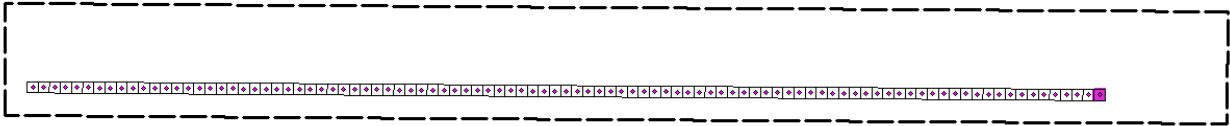


Figure 6 - Plan view of the numerical model set up. The dotted line corresponds to the model domain, and the grids correspond to the active cells in the model, which in this case is a single channel of cells, with a free overfall downstream boundary condition. Cell elevations were altered in order to achieve different slopes, and the water level was measured at the downstream end of the channel for comparison.

2.3.2 Results and Discussion

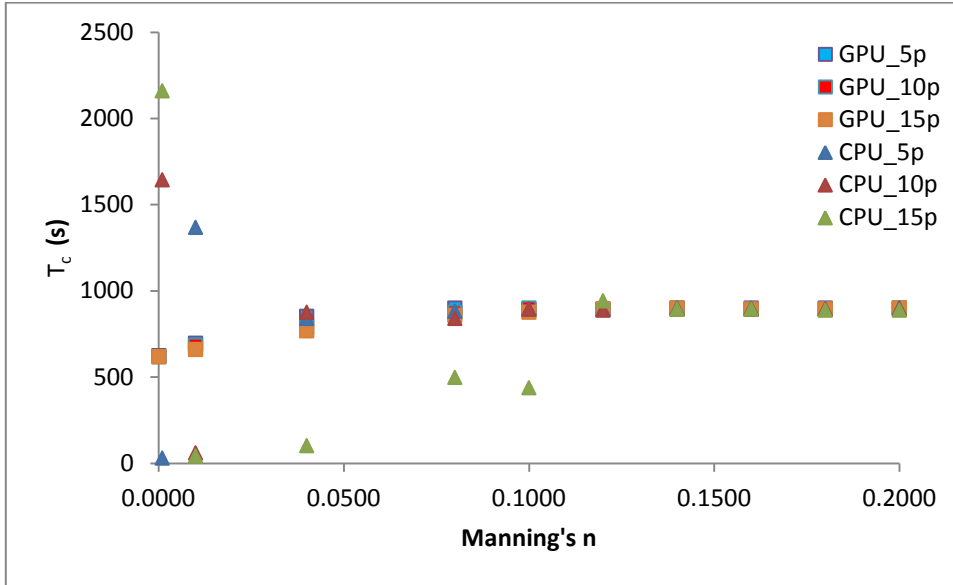


Figure 7 - Time of Concentration Vs. Manning's n, comparing the CPU and GPU solutions. A bed slope of 5%,10%, and 15% was graphed, and Manning's n was varied from 0 (frictionless) up to 0.2 (extremely rough). The title of "GPU_5p" corresponds to a TUFLOW GPU run at 5% bed slope and so on.

As evident in the above figure, TUFLOW GPU shows proportionality between time of concentration and bed roughness. At very low roughness and at very high slope, it is evident TUFLOW CPU has become unstable, most likely due a courant number above one from high velocities. As before mentioned, TUFLOW GPU has an adaptive RK4-5 time stepping method, allowing it to remain stable. This result validates TUFLOW GPU further, and demonstrates its inherent advantages over TUFLOW CPU.

3 Direct Rainfall Modelling Versus Hydrologic Models

3.1 Introduction

Traditionally, flood modelling has involved two stages as further discussed in Section 1 of this report. Firstly, the hydrologic modelling stage is undertaken to determine the quantity of water within a catchment during a given rainfall event using an excess rainfall hydrograph and routing it through the catchment, and secondly the hydraulic analysis where the mechanisms of flow along watercourses and across floodplains are defined (Caddis et al. 2008). Due to the inherent potential oversimplification of hydraulics in the hydrologic modelling phase, it is expected a direct excess rainfall model could make a beneficial replacement of the hydrologic model - especially if computational time is not sacrificed significantly.

A brief overview of hydrologic and *direct rainfall models* and their benchmarking is given based on their underlying mathematical framework. A critical review and analysis is undertaken of existing hydrologic models common to the Australian industry. The benefits and limitations of *direct rainfall models* and hydrologic models are addressed.

3.2 Hydrologic Model Benchmarking

Borah (2011) compared numerous hydrologic models which were capable of modelling runoff as a result of precipitation and the characteristics of soil and land covers, erosion of upland soil, and sedimentation. The speed and accuracy of 20 existing hydrologic models were compared with respect to routing procedures as they have the greatest influence on model performance. The level of physical accuracy is dependent on complexity of the mathematical formulations of the model, namely the hydrodynamic equations. A comparison was compiled as follows, where a model could be ranked on overland flow based on the physical origin of the equation (where the shallow water equations are considered to be the most physically based). It should be noted the shallow water equations are a very simplified version of the three dimensional Navier-Stokes equations. However for the purposes of this study, the shallow water equations are the most complex

equations available which are deemed suitable for hydraulic and hydrologic modelling of overland flow. The figure could be constructed as follows;

High Relative Physical Basis			Low Relative Physical Basis		
Shallow Water Equations	Diffusive Wave Equations	Kinematic Wave Equations	Nonlinear Reservoir Equations	Unit Hydrograph	Rational Method

Figure 8 - Comparison between different numerical methods for implementing a form of a hydrodynamic equation in accordance to Borah (2011).

This figure can be utilised as a framework for comparison of the physical basis of each numerical method for the remainder of the report.

3.3 Review of Hydrologic Models Commonly Used in Australia

There are a multitude of hydrologic models available in industry for use - URBS, RORB, XP RAFTS, and WBNM to name a few. All are very similar and can be encompassed under three main model types used to describe catchment and channel storage - which are basic, combined and split routing models. The basic model is where a representative stream length of the catchment and channel storage is assumed; the combined model is where the sub-catchment area and stream length is representative of the catchment and channel storage and the Split Model separates the channel and catchment storage components of each sub-catchment for routing purposes (Carroll 1998). Some may have an option choosing which model to use under certain circumstances. However, all storage components from each hydrologic software package is conceptually represented as a non-linear reservoir, which according to Borah (2011), is one of the least physically based methods as shown in

Figure 8. Methods which don't possess a high physical basis have room for potential error due to the over simplification of the actual physics which occurs in real life. The storage in these models is generally represented as follows;

$$S = k_c^1 Q^m \tag{3.1}$$

where S is the storage (m^3), k_c^1 (s) is the non-linear routing constant, Q is the outflow (m^3/s) and m is the catchment non-linearity parameter. The mathematical model implemented in each software package is extremely similar and is based on Australian hydrology literature. *Equation 1.1* has been expanded as an example, based on the URBS model recommendation for basic routing. It can be expressed as (Carroll 1998);

$$S = \left\{ \frac{\alpha \cdot f \cdot L \cdot n \cdot (1+F)^2}{\sqrt{S_c} \cdot (1+U)^2} \right\} Q^m, \quad (3.2)$$

where S is catchment storage (m^3/s), α is the storage lag parameter, f is the reach length parameter, L is the length of reach (km), U is the fraction of urbanisation of the sub-catchment, F is the fraction of sub-catchment forested, n is the channel roughness or Manning's n , S_c is the channel slope (m/m), Q is the outflow (m^3/s), and m is the catchment non-linearity parameter.

Non-linear reservoir routing is a simplistic method for modelling flow, and this may have adverse implications in terms of modelling accuracy in areas where topography doesn't significantly define the flow path or where little aerial photography is available. Each of the catchment parameters listed above simply alter the relationship between the storage and flow rate for each sub-catchment by a factor, which tends to oversimplify the model leading to a sacrifice in accuracy due to the heterogeneity present (Downer & Ogden 2004).

3.4 Motivation for Change in the Hydrologic Model Approach

The hydrologic model has made profound positive impacts in the applications of flood prediction, physically-based soil erosion models and reservoir engineering for the past 50 years (Downer & Ogden 2004). However, the lumped model approach used in Australian hydrologic models is overly simplistic and requires many assumptions which distort the hydrologic characteristics of a drainage basin (Borah 2011). Due to the heterogeneity in soil type, vegetation type, land use practices, and rainfall spatial and temporal variability – parameters required for flow routing and attenuation are typically averaged over an area, giving incorrect hydrologic characteristics at a catchment scale.

To prevent issues associated with heterogeneity of the catchment, hydrologic models are available which represent the entire catchment as a grid rather than a group of sub-catchments (Downer & Ogden 2004). However, these models also tend to be computationally expensive.

Grid-based (or distributed) hydrologic models have been developed since the 1990s, especially GIS-based hydrologic models (Liu & Chen 2008). Typically, the functions of GIS in hydrologic modelling are focused on spatial analysis and management of data, as well as visually displaying output. The effective use of GIS in hydrologic modelling has shown to alleviate the need to average catchment parameters as the topographic and hydrologic features can be extracted directly from the GIS interface. When compared with lumped models, grid-based models was shown to outperform the lumped models when rainfall and topography variability effects were significant (Koren et al. 2003).

A gridded hydrologic model designed by the National Oceanic and Atmospheric Administration utilises a kinematic wave model routing component with the water balance component modelled as a simple heterogeneous runoff process containing soil moisture information and six runoff components (Downer & Ogden 2004). The specific discharge at each grid cell is estimated using a channel parameterization equation, or as shown - the rating curve method as;

$$Q_{s,i} = Q_{s,o} \frac{F_i}{F_o} r_{A,i}^m, \quad (3.3)$$

Where F is the drainage area, r is a ratio of cross sectional area, Q is flow rate, and exponent parameter m is a constant equal to the estimated outlet value. The issue with using m is that the channel slope and roughness at upstream points is not considered (Koren et al. 2003), which may poorly represent the channel geometry if there are discontinuities in bed slope (e.g. transition from a flood plain to mountain ridge). Alongside this, the kinematic wave equation was implemented with a finite difference numerical method - which is not an effective discretisation method in the presence of many discontinuities as previously discussed in Section 2.1.1. Due to these reasons, it is more efficient to use a shallow water model as it is more physically based and has been validated for this study.

Aside from the advantage of using the SWEs to route flow through areas where poorly defined flow paths are prevalent, another major advantage of using *direct rainfall models* is for paleo-flood analysis. Sub-catchment interaction can be difficult to identify and quantify using commercial hydrologic software, and this may be an issue for low Annual Exceedance Probability events when significant interaction occurs between sub-catchments and flood plains - resulting in an underestimation of the flow (Kuczera 1999). The use of *direct rainfall models*

reduces the chances of this occurrence with the GIS based system using Digital Elevation Models to route the flow.

3.5 Direct rainfall modelling

Direct rainfall modelling techniques have only been considered as a feasible hydraulic modelling technique recently. As a result, it is largely untested and its limitations aren't yet fully understood. Common issues have come to light associated with model losses, run-times, grid issues, and very shallow flow (Hall 2014). Some of the key limitations of *direct rainfall modelling* can be identified as (Hall 2014; Rehman 2011);

- Shallow flows (generally experienced upstream) may have a mean hydraulic depth much smaller than deemed suitable for application of Manning's roughness parameters.
- The approach requires high quality Digital Elevation Models (DEM), and drainage channels may need to be embedded due to a coarse grid.
- It is difficult to represent the sub-grid drainage infrastructure, where some water is trapped upstream when it would ordinarily runoff due to sub-grid infrastructure - causing a delay in hydrograph response.
- The model grid size affects flood extent, magnitude and flow paths. The same grid dimensions should be used in calibration and in scenario situations - which may limit some models.
- The high grid cell count in *direct rainfall models* increase run-time significantly (although this limitation is less relevant to GPU models).
- Appropriateness of several rainfall loss methods.
- There is a general lack of guidance in comparison to the well established hydrologic models.

Some of the above issues have the potential to be solved quite easily (such as implementing a code to shift puddles of water to regions which would allow it to runoff as it would in reality to prevent the underground drainage infrastructure dilemma) - however some of the other listed limitations require more in depth research.

In the above list the author identifies the two most significant issues to be related to modelling the flow at small mean hydraulic depth, and the effect of grid size. Appropriateness of rainfall loss

methods are also significant but have been previously explored (Caddis et al. 2008). Hence, the author will firstly review existing research conducted into the effect of grid size in *direct rainfall modelling*. The conduct further research into the applicability of hydraulic resistance equations (Clark 2008; Muncaster 2006).

3.5.1 Effect of Grid Size

A fundamental concept on the effects of spatial variability with scale was first defined by Wood et al. (1988), who introduced Representative Elementary Area (REA). The REA defines a point where variability can be integrated over an area large enough such that effects of the small scale variability may be attenuated. Watershed characteristics including rainfall, topography and rainfall variability can be represented by various length scales with the most accurate model results yielded when the REA has a length scale greater than the length scale of rapidly varying hydrologic components, but less than the length scale of slowly varying hydrologic components (Wood et al. 1988). It was concluded that the REA is strongly influenced by the topography, with length scale of rainfall only playing a secondary role in determining the REA size.

It follows that grid size needs to be small enough to diminish significant model variability, but large enough to reduce computational run time. This is less of an issue for models running on GPU processors as before mentioned. However, due to the fact that TUFLOW GPU does not utilise a flexible mesh (i.e. discretised grid which may vary in cell size spatially), or does not yet contain a coupled 1D-2D model - drains often need to be stamped onto the grid through the use of an artificial topography layer. This practice can cause overestimation of the hydraulic capacity of the drain (as the grid size is quite often wider than the drain, resulting in an interpolation between the original 2D layer and the altered 2D layer giving a larger cross sectional area of the drain than actually occurs in reality) (Rehman 2011).

Two dimensional hydraulic models, TUFLOW (Syme 2006) and SOBEK (Anonymous 2007) were tested as hydrologic models by their ability to reproduce the same direct runoff flow hydrograph as a well calibrated WBNM model when grid size was altered (Clark 2008). SOBEK exhibited an inverse proportional trend between peak flow rate and grid cell size; with TUFLOW displaying a proportional relationship between peak flow rate and grid cell size. As cell size decreased, both models converged to WBNM estimates.

Hence, a suitable grid size must be chosen for the hydraulic model to ensure the REA is satisfied and to avoid excessive computation time. Digital stamping for topography change should also be undertaken with caution. Using this as a basis, the *direct rainfall model* can be compared with an existing hydrologic software package and benchmarked.

3.5.2 Procedure - Comparison of Direct Rainfall Models and Hydrologic Models

A comparison between *direct rainfall models* and hydrologic models can be undertaken most effectively using a gauged catchment for a real flood event in a real catchment. The shape and magnitudes of the output hydrographs of the hydrologic and *direct rainfall models* can be compared and gauged against the real life data.

The test catchment is situated in Durrumbul, New South Wales. The catchment is approximately 40 square kilometres in size and contains slopes up to 15%. Dominant flow paths are created from various mountain ranges present on the catchment. The land use is predominantly bushland, ranging in density from 'open plan with tree patches' to 'forest'. No buildings exist.

A breakdown of the catchment is presented in

Figure 10 which details the layout of the catchment and also demonstrates the sub-catchment delineation. The chosen hydrologic model of choice is XP RAFTS due to the accurate results achieved by Adams (1991) on a real catchment compared to other hydrologic software used. The chosen hydraulic model is TUFLOW GPU because it supports direct excess rainfall GPU models, and also due to the validation of BMT WBM's software being a partial goal of this thesis.

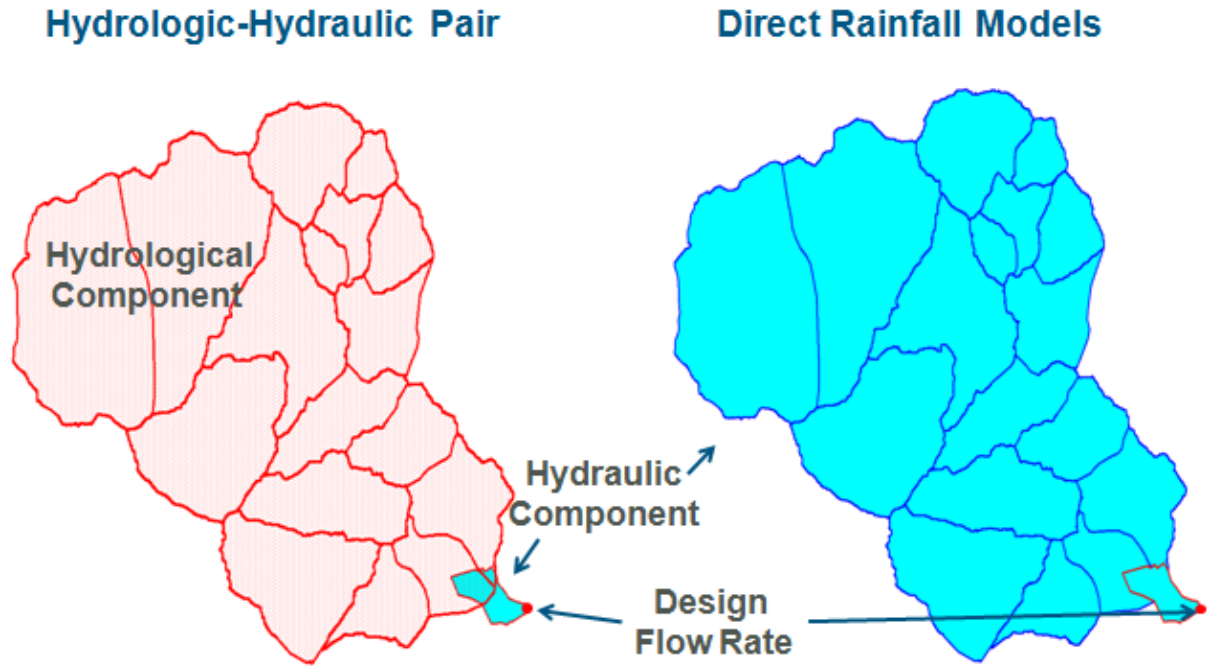


Figure 9 – Relative model set-up comparison between RAFTS hydrologic model and TUFLOW GPU hydraulic model on gauged catchment in North Byron.

A stream gauge is located at the downstream end of the catchment, directly preceding the 'design flow rate' point of the catchment presented above. A storm event occurred over the period 25/01/2012-26/01/2012 in which all total rainfall for each sub-catchment was recorded. The model specifics are presented in Appendix 4.

3.5.3 Results and Discussion

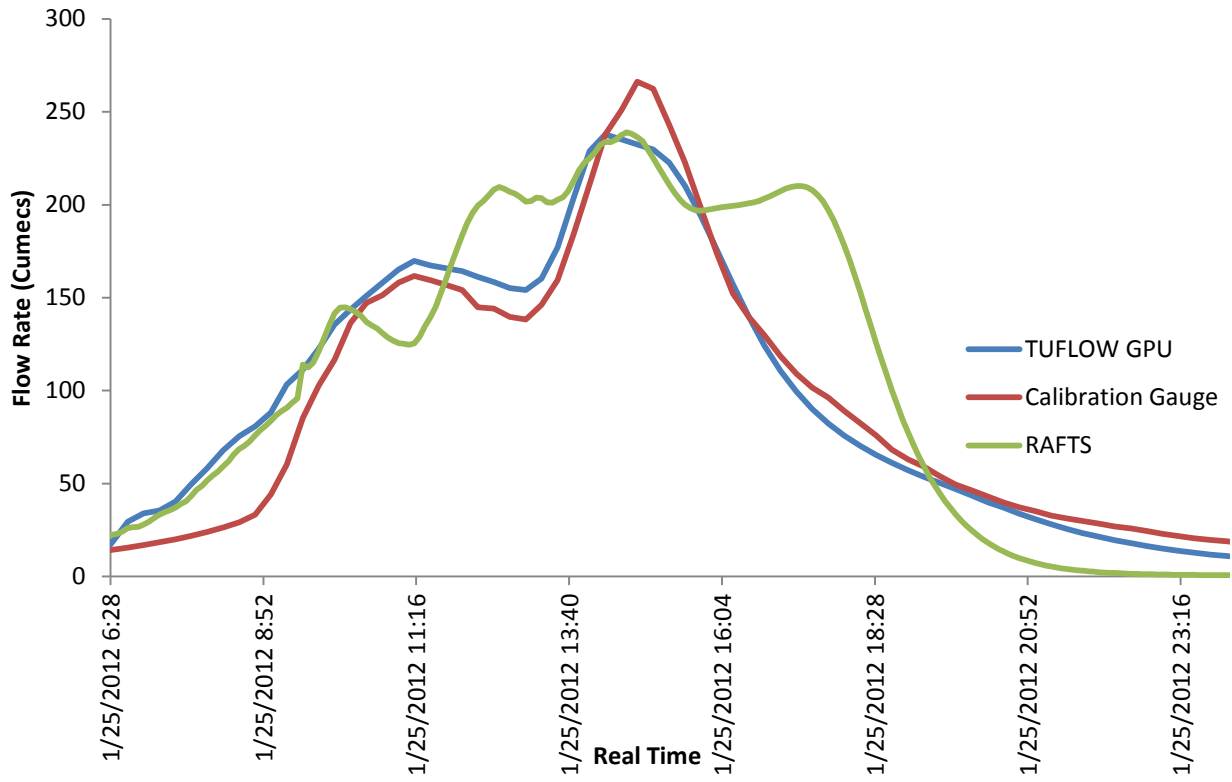


Figure 10 - TUFLOW GPU versus RAFTS for the gauged catchment in North Byron

Curve Characteristic	TUFLOW GPU	XP RAFTS
Rising Limb	x	x
Timing of First Peak	✓	x
Magnitude of First Peak	✓	x
Timing of Second Peak	✓	✓
Magnitude of Second Peak	x	x
Falling Limb	✓	x

Table 2 – Summary of Figure 11, breaking up the *Calibration Gauge* curve into characteristics, and determining whether each numerical model accurately represents this characteristic in their results.

As evident in

Figure 10 and Table 2, the hydraulic model has a more correct shape with respect to magnitude and timing when compared to the gauge data as the timing of the first and second peaks are matched more closely. However, neither methods are able to match the gauge data exactly, as the peak flow rate is underestimated by approximately 1%. The hydrologic model estimates the same peak flow as the hydraulic method, but the shape of the curve is less accurate and the first peak is missed. Assuming the gauge data is error free, the reasons for these discrepancies in the hydraulic model are most likely due to the incorrect specification of soil infiltration losses which result in the overestimation in flow rate at the rising limb of the hydrograph.

The Muskingum method is utilised in RAFTS to route flow along the catchment length which is an implementation of a non linear reservoir equation. Analysis by Borah (2011) showed this method to be less complex and less physical than the shallow water equations. The Durrumbul catchment has abrupt topography change, steep slopes and poorly defined flow paths, which makes it particularly hard for a hydrologic model to accurately reproduce (especially for poorly defined flow paths). Poorly defined flow paths and abrupt topography change are expected to be the primary reasons for the hydrologic model's inaccurate representation of the historical event, especially in capturing the first peak of the hydrograph where flow paths are still being established. The overestimate of flow rate initially is likely to have occurred from incorrect

specification of soil infiltration losses. Considering the land use of the catchment is reasonably diverse, it is expected the inability of the hydrologic model to capture the falling limb of the hydrograph is likely to be from the lumping of roughness terms; as the water mass is not leaving the model domain fast enough.

In terms of weighing up the trade-offs between model set-up time/complexity, model accuracy, and model run time, the following can be concluded;

- In order to capture the shape of the hydrograph correctly, methods adopted by hydrologic models aren't complex enough in this situation to capture the precision or accuracy that a hydraulic model can.
- Hydrologic models and hydraulic models take approximately the same time to set up, dependent on the work required on the digital elevation model for the hydraulic model. More degrees of freedom to adapt the topography are available in *direct rainfall models* which can be an advantage.
- The computation time on hydrologic models are at least an order of magnitude faster. Depending on the desired model speed, hydrologic models can still estimate to a reasonable degree of accuracy the flow rate and thus may be preferred. Until GPU cards advance much further than they have at present, running speeds for the hydraulic model are not competitive in comparison to hydrologic model run speeds.

Due to the fact the catchment was unsophisticated and reasonably homogeneous in terms of land use (and was not urbanised), a fairly low level analysis was performed. It is recommended more research is pursued into the sophistication (size and drainage features etc.) of different types of catchments and how it may affect hydrologic and hydraulic models.

4 Shallow Flow Hydraulics

Shallow flows are experienced frequently in *direct rainfall models*, in which effective shallow flow modelling techniques have yet to be developed. Shallow flow conditions are defined as those where the flow depth is of the same order of magnitude as the bed material roughness height, and is characterised by high flow resistance, presence of flow separation and rapid turbulent velocity fluctuations (Jordanova 2008). This makes the flow extremely difficult to model, and makes it vital for the underlying flow regime to be well understood such that it may be modelled with a higher degree of accuracy.

Shallow flow hydraulics may either be characterised by large scale or intermediate scale roughness, dependent on the depth of flow and roughness height of the bed material. Roughness scale was determined for a gravel creek bed based on the following classifications (Bathurst et al. 1981; Bray & Davar 1987; Jordanova 2008):

- $\frac{d}{k_s} < 1.2$ - Large scale roughness,
- $1.2 < \frac{d}{k_s} < 4$ - Intermediate scale roughness,
- $\frac{d}{k_s} > 4$ - small scale roughness.

Where d (m) is the mean hydraulic depth of the flow, and k_s (m) is the bed roughness height. Roughness scale is a fundamental concept and will be used as the framework to determining the most suitable method of modelling shallow flow.

The following sections contain an overview of the mechanisms of flow resistance, a brief history of velocity distribution modelling, a review of some important literature on shallow flow and roughness scale, numerical modelling at large scale roughness, and analysis of experimental shallow flow data to determine the most suitable modelling technique. The most suitable method will be implemented into TUFLOW GPU and utilised in a model of a real life catchment to determine its practicality.

4.1 Mechanisms of Flow Resistance

Two fundamental properties underpinning flow resistance is flow regime and whether the mass of water obeys equilibrium. The four main components contributing to flow resistance in open channel flow are the following (Yen 2002):

- Skin friction,
- Form resistance and drag,
- Wave resistance (although less relevant at shallow flow), and
- Flow unsteadiness.

With respect to hydraulic resistance, flow regime determines the relationship between mean velocity and piezometric pressure gradient (which is the friction slope for open channel flow), through the change in shear distribution over the depth of the fluid body (for skin friction dominated resistance)(Crowe 2009). Hence, it is trivial the velocity distribution will be affected with a change in flow regime.

4.2 The History of the Development of Velocity Distribution

The fluid velocity formula for uniform flow was actually first developed in 1768 by Antoine Chèzy, who proposed:

$$\frac{\bar{V}}{u_f} = C , \quad (4.1)$$

where C is Chèzy's coefficient (which is a constant), \bar{V} is mean velocity (m/s) and u_f (m/s) is the friction velocity. This proposition needed more consideration into Chèzy's coefficient, which was dependent on material roughness and the mean hydraulic depth, such that the formula was revised by Phillippe Gauckler in 1867. Gauckler's equation was later redeveloped by Robert Manning in 1890, who proposed:

$$\frac{\bar{V}}{u_f} = \frac{d^{1/6}}{n} \quad (4.2)$$

where n is Manning's coefficient (Dingman & Sharma 1997). Whilst this is a good approximation, it assumes uniform flow conditions and that the bottom slope is the same as the slope of energy grade line and water surface slope.

The main downfall of this equation is that the Manning's n coefficient is physically meaningless.

With units of $\frac{L^{1/3}}{T}$, the coefficient does not translate to anything physical and is simply a correctness factor. A more accurate, more rigorous solution was developed in 1930 by Theodore Von Karman, who gave the normalised version of his equation as

$$\frac{V}{u_f} = \frac{1}{\kappa} \ln \left| \frac{z}{z_0} \right| \quad (\text{Von Karman 1975}), \quad (4.3)$$

where z_0 is dependent on flow regime, but is a function of u_f , k_s and ν - where k_s (m) is the roughness height, d (m) is the mean hydraulic depth, κ is Von Karmen's Constant and ν (m²/s) is the kinematic viscosity.

4.3 Studies Undertaken on Manning's n

The Manning formula was derived empirically in 1890 by Robert Manning, who actually proposed two formulae (Yen 1992);

$$\frac{\bar{V}}{u_f} = C \left[1 + \frac{0.22}{\sqrt{mR_h}} (R_h - 0.15m) \right] \quad (4.4)$$

$$\frac{\bar{V}}{u_f} = \frac{d^{1/6}}{n} \quad (4.5)$$

where m is the atmospheric pressure measured in height of mercury, and $C = \frac{1}{n}$ where n is Manning's coefficient.

He realised equation (4.5) was dimensionally inhomogeneous and incorrect and republished a paper in 1895 only displaying equation (4.4) which was dimensionally more homogeneous, but was not adopted by others (Yen 1992). C is recognised by most as $\frac{1}{n}$ where n is the material roughness. It is also important to note equation (4.4) is a better estimate of the velocity distribution than equation (4.5), but is still not correct and better estimates exist.

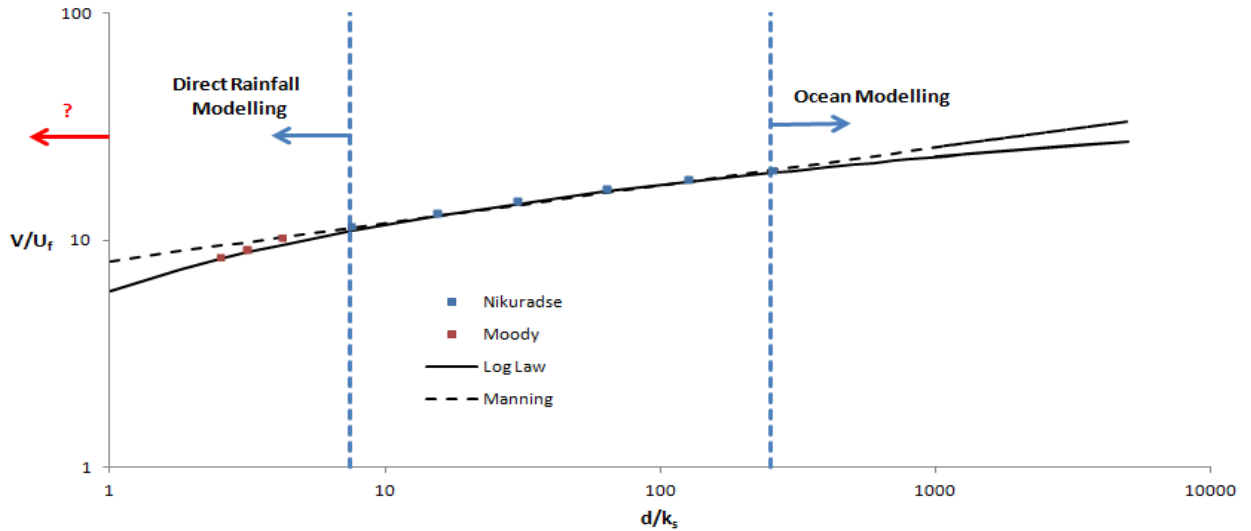


Figure 11 - Relative accuracy of Manning's equation based against experimental data (Nikuradse 1950). Data is graphed using normalised mean velocity (which is normalised with the friction velocity) on the Y axis and relative submergence on the X axis.

As apparent in Figure 11, through investigation of Manning's equation it is evident for the most common roughness range (approximately $10 \leq \frac{d}{k_s} \leq 250$ taken from the Moody diagram (Crowe 2009)), $V \sim d^{2/3}$ meaning n is independent of depth. However, for shallow flows this ratio violates the lower bounds, where Manning's equation is no longer valid due to the prevalence of intermediate or large scale roughness effects (Jordanova 2008). When relative submergence, $\frac{d}{k_s}$ lies between 1 and 4, the roughness scale may be classified as intermediate roughness (Bathurst et al. 1981). As mentioned in Section 1, intermediate and large scale roughness are best represented by a contribution of drag friction, turbulent eddies, and skin friction; as opposed to small scale roughness which can be accurately represented by skin friction alone. Literature must be explored to determine the behaviour of Manning's equation under shallow flow hydraulic conditions.

Kibler (1991) conducted experiments using artificial rainfall simulators to determine the relationship of Manning's n with depth for sheet flow on Portland cement concrete surfaces using kinematic wave theory; resulting in the empirical relationship:

$$n = 0.2887d^{-1.63}, \quad (4.6)$$

where d is the depth of water in metres. The data was collected for depths in the range of 1-2 millimetres, with the roughness height of the Portland cement measured as 546 micrometres; giving a roughness scale of $1.8 \leq \frac{d}{k_s} \leq 3.8$. This is in the intermediate roughness scale. No drag is considered in this case as the Manning's value is simply lumped and changed with depth. This does not emulate the physical process and given the limited range of depths measured and may not be very practical for implementation in the numerical model, although consideration may still be given to the results.

It is also required to understand the flow characteristics on vegetated slopes for rural catchments as this is more common in hydrologic modelling which is the primary investigation of the hydraulic model as discussed in Section 1.

The relationship for flow on vegetated slopes can be expressed as $S = f(\mathbb{R}, \mathbb{F}, S_w, \frac{k_s}{R_h}, L_v, J, \frac{d}{k_s}, M)$, where S is the storage, S_w is the energy slope, J is vegetation flexibility, L_v is representative geometry measure, M is density distribution on channel bed, \mathbb{F} is the Froude Number, and $\frac{d}{k_s}$ is the relative submergence (Yen 2002). The complexity involved makes it difficult to define the velocity distribution and to determine the exact relationship between all variables.

The limited application of Manning's equation on vegetated channels has been realised for a significant period of time, where the following issues were noted (Turner & Chanmeesri 1984):

- Manning's n varies significantly with depth which violates interpretation of the equation as previously discussed in Section 4.3.
- The mean hydraulic depth becomes an issue as vegetation increases to a point where flow through the cross sectional area is analogous to flow through porous media.
- A fixed exponent for the mean hydraulic depth implies sheet flow always behaves in turbulent conditions; where flows in this instance are likely to be developing flows as the regime fluctuates between laminar and fully turbulent.

Research shows it is highly unlikely the Manning equation is applicable to these kind of conditions (Yen 2002). Many attempts to reproduce a workable solution for hydrodynamic flow in vegetated channels have been tried, with the majority using two main procedures:

- a. Developing prediction equations based on empirical procedures.
- b. Reusing Manning's equation and making small adjustments to better fit their experimental data.

However, both of these methods explain very little about the physics behind shallow flow in vegetated channels so their results are not a significant finding.

A review of the suitability of flow equations/hydraulic resistance for surface irrigation flows gives insight into finding a suitable method of modelling hydraulic resistance for shallow flow through. Depths in surface irrigation are typically less than 150mm, and the velocities of flow are between 0.2 and 0.4 m/s, giving the flow a low mean hydraulic depth - though the flows may be a mix of laminar and turbulent flows (Maheshwari 1992). Raudkivi (1963) showed that the lower bound of Manning's n is approximately limited by $\frac{d}{k_s} = 30$ where d is the depth of flow and k_s is

the equivalent roughness height. If Manning's equation is to be adjusted, it was concluded that the exponent of hydraulic radius in the Manning equation should be varied dependent on the value of $\frac{d}{k_s}$. Hence empirical equations developed in turbulent flow conditions may give erroneous

results when applied to shallow flows on vegetation.

Development of empirical equations on shallow flow been shown to violate physical and dimensional principles. An example is a study undertaken by Garcia Diaz (2005), in which an approximate method was derived to calculate the hydraulic resistance for small-depth flows on vegetated beds, where experimental results showed dependence of Manning's coefficient on roughness height, flow depth, and bed slope (Garcia Diaz 2005). The Manning equation; previously depicted in this report as

$$\frac{\bar{V}}{u_f} = \frac{d^{1/6}}{n}, \quad (4.7)$$

can be represented as a function of the Froude number:

$$\mathbb{F} = \frac{\bar{V}}{\sqrt{gd}} \quad (4.8)$$

by acknowledging gravity is the dominant force in the momentum component of the Shallow Water Equations. It follows that

$$n = \frac{d^{1/6} S^{1/2}}{g^{1/2} \mathbb{F}} \quad (4.9)$$

where the author sets the framework of his methodology by proposing

$$n = a \mathbb{F}^{-b}, \quad (4.10)$$

where a and b are empirical coefficients derived using experimental data. However, the author unnecessarily outlines an iterative process using equations (4.10) and (4.9), and continuity principles to calculate the fluid depth and velocity when the Manning coefficient converges to one value. The same result can be obtained using an analytical solution as:

$$d = \left(\frac{aq^{(1-b)} g^{b/2}}{s_0^{1/2}} \right)^z, \text{ where } z = \frac{1}{5/3 - 3b/2} \quad (\text{Jarvela \& Aberle 2007}). \quad (4.11)$$

Since Manning's n has dimensions of $s m^{-1/3}$, and the Froude number is dimensionless, equation (4.10) states that the coefficient a must have the same dimensions as Manning's n . It follows from equation (4.11) that $b=1$ (for dimensional correctness) to yield the following;

$$d = a^6 g^3 S_0^{-3}, \quad (4.12)$$

suggesting depth is independent of discharge which is realistically incorrect (Jarvela & Aberle 2007). The author has derived values for $b \neq 1$, which does not satisfy dimensional correctness. The approach is not physically sound and hence will not be considered in the methodology of this report.

Empirical equation development may be useful for situations where probabilistic methods are required to correctly model shallow flow. A good example is shallow flow on an erosion bed. Energy is required to move the soil medium and will impact on the momentum component of the SWEs. This is difficult to model, in which case empirical studies can prove useful. A study undertaken on erodible material has shown Manning's n value to increase with increasing slope. Various slopes and materials were tested using a regulated discharge and dye tracer to measure velocity on Cropland, Fallow, Orchard, Woodland and Wasteland land uses (Hessel et al. 2003). Observations showed that this was primarily due to flow concentration causing erosion on steep

slopes thus decreasing the mean hydraulic depth. Velocity did not increase with bed slope angle, which can be explained in the increase in erosion rate with slope angle (Gimenez & Govers 2001); causing an increase in bed roughness and hence negligible velocity increase. It follows that material subject to erosion should use the empirical formula

$$\bar{V} = 3.52Q^{0.294} \quad (4.13)$$

developed by Gimenez and Govers (2001), or a different approach entirely should be adopted (such as using the log law). No relationship between Manning's n and slope was found for non erodible material (i.e. Woodland). This study may be useful for finessing TUFLOW GPU as a hydrologic model for sub-catchments with steep erodible material. However, these results may be limited in their application given that some energy is expended into moving erodible soil such that hydraulic equations derived from first principles (such as the energy equation) would be difficult to model.

A more physical approach was undertaken for the interaction between reeds and river morphology with shallow flow hydraulics by James (2002). A mean velocity formula was developed considerate of drag forces and skin friction. The proposed equation was:

$$V = \frac{1}{F_f} S^{1/2}, \text{ where } F_f \text{ is:} \quad (4.14)$$

$$F_f = \frac{1}{\sqrt{\left(\frac{1 - \frac{N\pi\phi^2}{4}}{\frac{f}{8} + \frac{1}{2}C_D Nd\phi} \right)} gd} . \quad (4.15)$$

where f is the Darcy Weisbach friction factor, C_D is the stem drag coefficient, N is the number of stems, d is water depth, and ϕ is the average stem diameter. The method behind the derivation of equation (4.15) is robust and will be considered in this study.

Equation (4.15) was found to match the experimental data well for flow beneath the reed stem. The following points of the experimental study were concluded (James 2002);

- Flow resistance depends strongly on stem density and drag coefficient but not independently on channel or slope.

- The velocity profile of the submerged flow was essentially uniform. However, the flow above the stem tops was found to have a velocity distribution which could be modelled accurately with a bed shear formula, such as *The Law of the Wall*. This law will be discussed further in Section 4.5.
- Conveyance is significantly affected by the distribution pattern of the reed beds. Manning's n was found to vary strongly with flow depth. If the longitudinal distribution of the reeds is continuous, resistance was shown dependent on the number of stem-water interfaces. If they were longitudinally discontinuous, the problem becomes more complex, with strong dependences on areal coverage, distribution pattern, and patch size and shape. More research is required in this area.

This concept was further explored by Sharpe and James (2007), who investigated hydraulic resistance at large scale roughness as a part of a sediment deposition study using rigid dowel as model reed stems; to determine the most suitable modelling method for flow through reeds at shallow depth. It was found that Manning's n was found to increase with stem density and depth. However, when equation (4.15) was used, the predictions collapsed to show independence of depth as shown in Figure 12. This provides a good basis for the use of F_F rather than Manning's n for drag dominated flows. This method will be given consideration for large scale roughness conditions.

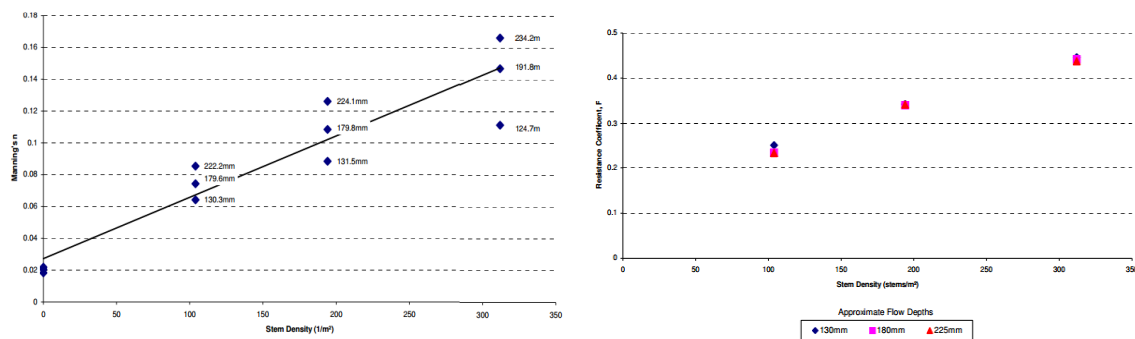


Figure 12 - Comparison of Manning's n and F , graphed with stem density on the X axis and Manning's n /James' F on the Y axis. Manning's n plot on the left shows significant scatter with depth and James' F on the right shows a collapse in data points (Sharpe & James 2007).

The most useful study available in terms of data was that executed by Jordanova (2008). Hydraulic resistance at small, intermediate, and large roughness scale was investigated in a

laboratory flume with varying sized hemispheres glued to the channel bed and varying the depth to procure data at different values of $\frac{d}{k_s}$ to determine the following (Jordanova 2008):

- Density of roughness elements cause profound impact on hydraulic resistance, with hydraulic resistance proportional to element density at all roughness scales.
- Higher overall flow resistance was experienced for milder slopes than for steeper slopes.
- Arrangement of roughness elements only influences resistance significantly when $\frac{d}{k_s} < 1$, for which continuous flow paths (parallel arrangement) decreases flow resistance more than staggered arrangement.
- There is a definite change in physics for hydraulic resistance between intermediate roughness scale and large roughness scale elements and require different methods to model these changes.
- Flow resistance is a maximum at $\frac{d}{k_s} = 1$, and decreases rapidly for deeper flows and gradually for shallower flows.
- Roughness element height, arrangement density, arrangement pattern and variability of element size are significantly more pronounced for large roughness scale conditions than for small or intermediate scale.

Hydraulic resistance was measured using the Darcy Weisbach friction factor and results are presented on the basis of equilibrium flow. A relationship between the friction factor and relative roughness was determined, however was analysed incorrectly. For given patterns with varying roughness heights it is incorrect to base the relative roughness on the largest roughness element. Rather, the most correct way to model k_s is through the relationship $k_s = k_{RMS}$, where k_{RMS} is the root mean square of all roughness elements (Allen et al. 2007). An example calculation is performed in Appendix 6.

4.4 Procedure for Large Scale Roughness Testing

Studies undertaken by Sharpe and James (2007) determined the most physical relationship through emergent reed flow to be;

$$\bar{V} = \frac{1}{F_f} S^{1/2}$$

$$F_f = \frac{1}{\sqrt{\left(\frac{1 - \frac{N\pi\phi^2}{4}}{\frac{f}{8} + \frac{1}{2}C_D Nd\phi} \right) gd}}$$

At present without adjusting the source code, TUFLOW uses the Manning equation to estimate mean velocity. A representative Manning's n which encompasses drag force and bed shear, n_* , can be determined by equating the mean velocity of emergent reed flow with the mean velocity of Manning's equation. That is;

$$\bar{V}_f = \frac{1}{F_f} S^{1/2}$$

$$\bar{V}_{Manning} = \frac{1}{n_*} d^{2/3} S^{1/2}$$

$$\bar{V}_{Manning} = \bar{V}_f$$

$$\therefore n_* = d^{2/3} F_f$$

$$n_* = \frac{d^{1/6}}{\sqrt{\left(\frac{1 - \frac{N\pi\phi^2}{4}}{\frac{f}{8} + \frac{1}{2}C_D Nd\phi} \right) g}}$$

It is evident this variable varies with depth, stem density, bed roughness, stem diameter, and drag coefficient. Considering all other variables except depth are fixed in this situation, a Manning's n varied with depth file must be constructed to capture the correct synergy of bed shear and drag force within the model.

The experiment was carried out in a 0.38m wide, 15m long flume with slope varying from 0.1% to 0.2%. A rubber matt with tufts 0.03m in length was placed along the channel bed, and stiff

plywood was placed as an imitation for the emergent reeds. Constant flow rate was applied at the flume entry and was varied until normal depth was achieved. This was measured using a V-notch weir in the experiment.

These conditions were imitated in TUFLOW using the same channel dimensions and a representative Manning's n as the bed roughness. The TUFLOW files can be found in Appendix 6. TUFLOW model values can be summarised as follows:

Model Run Number	Flow Rate (m ³ /s)	Stem Density (stems/m ²)	Bed Slope
1	8.56	104	0.0019
2	12.95	104	0.0019
3	16.11	104	0.0019
4	8.51	194	0.0019
5	6.42	194	0.0019
6	10.92	194	0.0019
7	8.59	312	0.0019
8	4.6	312	0.0019
9	7.2	312	0.0019

Table 3 - Model conditions in TUFLOW for large scale roughness modelling.

4.4.1 Results and Discussion

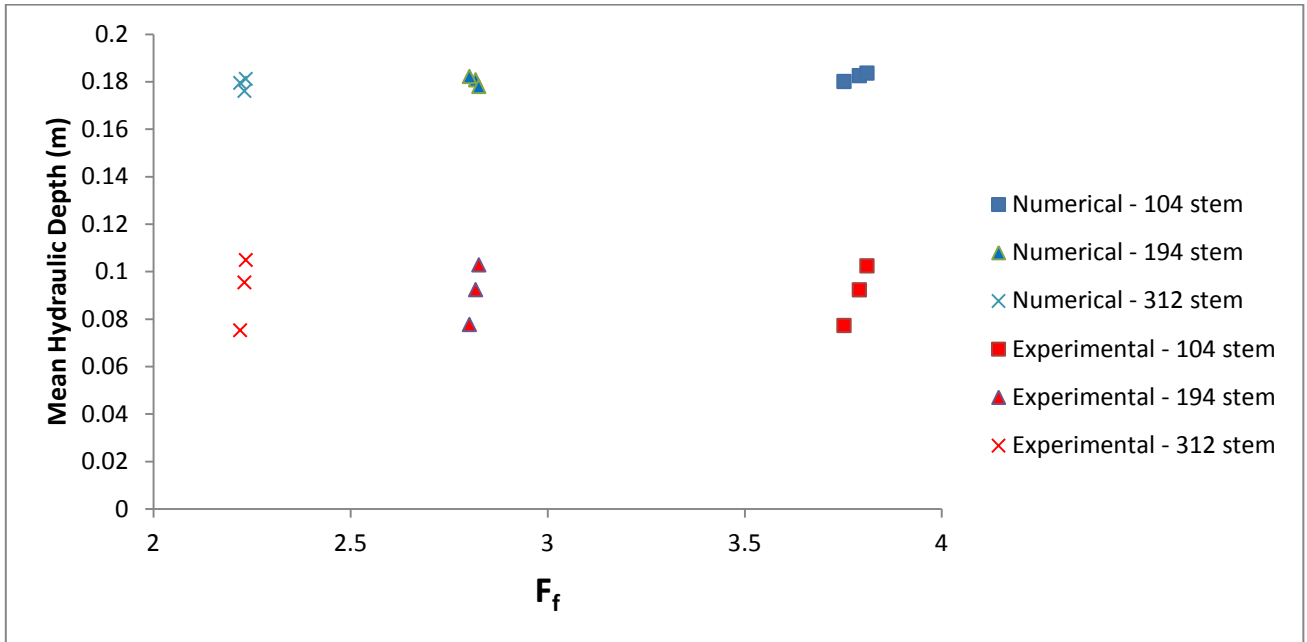


Figure 13 - Numerical results for the 'Emergent Reeds' experiment using the 'Experimental Depth Measurement' as a downstream boundary condition

As evident in Figure 13, specification of a representative Manning's n based on the methodology in Section 4.4 is insufficient to correctly simulate large roughness conditions. Given the complexity of large scale roughness conditions, this result is expected. In order to correctly model large scale roughness conditions, the appropriate synergy of bed shear, drag force and secondary flows must be captured. Considering this, the methodology shows negligence to any existence of secondary flows, and has evidently captured the physics of drag force incorrectly. The methodology outlined by Sharpe and James (2007) evidently requires more critical thought into the drag component of large scale roughness conditions, pattern effects in particular. That is, the derivation of equation (4.15) assumes a lumped stem density, but the arrangement of stems will impact on the flow pattern and thus the velocity distribution. This can be shown as follows;

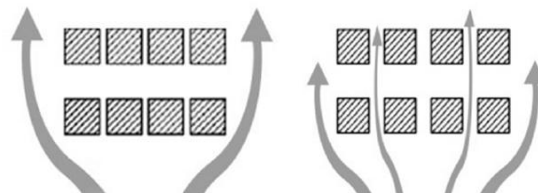


Figure 14 – Example of the impact of element arrangement in large scale roughness conditions on the flow pattern.

Because flow patterns change based on element arrangement, pressure distribution within the elements will change (which can be illustrated through a flow net etc.) which means the velocity distribution must change according to the Bernoulli equation. The effect of patterns on velocity distribution needs to be addressed to determine a suitable method to model large scale roughness conditions. More intensive testing (such as wind tunnel testing) could be explored to determine the wake properties (and thus understand secondary flows).

4.5 The Law of the Wall (Logarithmic Velocity Law)

For overland flow, the most physical method to define the resistance for skin friction dominated flows is through a turbulent boundary layer. A boundary layer is defined as the flow region next to a solid boundary in which the flow field is affected in its presence (Chanson 2014). It initiates from the 'no slip' condition at the boundary, in which the layer of fluid directly adjacent to the boundary has a theoretically 'zero' velocity, and adjacent to this layer is the fluid travelling at free stream velocity. The impossibility of this infinite velocity gradient is met by a layer of fluid over which the velocity transitions from the 'no slip' condition to the free stream velocity, which is termed the boundary layer. Furthermore, the turbulent boundary layer can be broken down into three regions;

1. The *viscous sublayer region*, where viscous stresses are high and turbulent stresses are small.
2. The *wall region/turbulent zone*, where viscous stresses are small and turbulent stresses are large.
3. The *outer region*, which occurs just outside of the outer edge of the boundary layer.

A summary of the pertinent boundary layer equations for a smooth plate (no pressure gradient) is given below as a combination of the material presented in literature.

Application	Equation	Approximate Ranges	Sources
Velocity – Inner Wall Region	$\frac{V}{u_f} = \frac{u_f z}{\nu}$	$\frac{u_f z}{\nu} < 5$	Chanson (2009) Popovich and Hummel (1967)
Velocity - Logarithmic Region	$\frac{V}{u_f} = \frac{1}{\kappa} \ln \left \frac{u_f z}{\nu} \right + 5$	$30 < \frac{u_f z}{\nu} < 500$ $\frac{z}{\delta} < 0.15$	Crowe et al. (2009) Chanson (2009)
Velocity - Defect Region	$\frac{V}{u_f} = \frac{V_0}{u_f} + \frac{1}{\kappa} \ln \left \frac{z}{\delta} \right $	$\frac{z}{\delta} > 0.15$	Chanson (2009)
Velocity – Power Law $[\frac{1}{7}]$	$\frac{V}{V_0} = \left(\frac{z}{\delta} \right)^{1/7}$	Entire Layer	Schlichting et al. (2000) Chanson (2009)
δ – Power Law $[\frac{1}{7}]$	$\delta = \frac{0.16x}{\mathbb{R}_x^{1/7}}$	-	(Crowe 2009)

Table 4 - A summary of equations which can be applied in the regions of the boundary layer where δ (m) is the boundary layer thickness and z (m) is the height above the solid boundary, and V_0 is the free stream velocity.

It is evident the wall region encompasses the largest flow region based on the approximate range of

Table 4, hence this is the most useful region to model the velocity distribution with. This can be achieved through the *Law of the Wall*.

The *Law of the Wall* describes the velocity in the flow zone outside the viscous sublayer or theoretical zero logarithmic velocity point, and can be derived by noting the conceptual diagram in Figure 15, where flow of depth d moves downstream over sand grains of roughness height k_s .

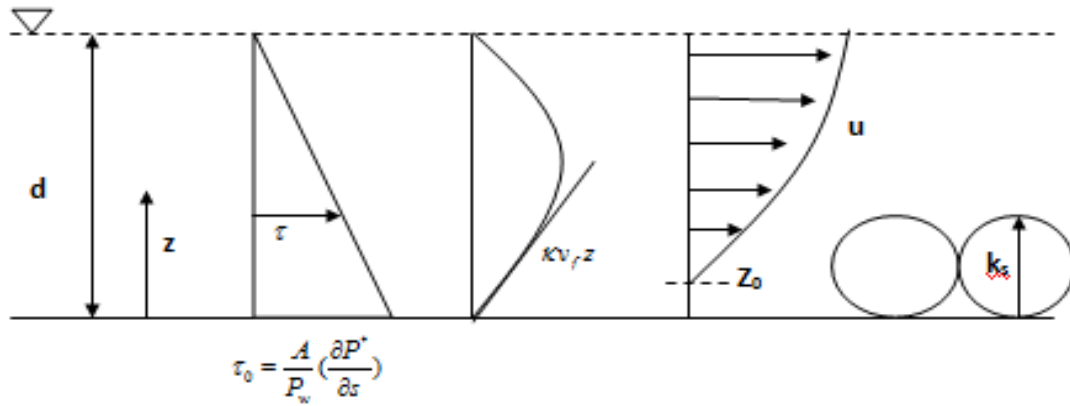


Figure 15 - Concept of The Law of the Wall

The velocity u changes over height z as follows;

$$\frac{\partial u}{\partial z} = \frac{\tau}{\rho \nu_t} = \frac{\tau_0 \left(1 - \frac{z}{d}\right)}{\rho \kappa z \left(1 - \frac{z}{R}\right) \sqrt{\frac{\tau_0}{\rho}}} = \frac{1}{\kappa} \cdot \frac{1}{z} \sqrt{\frac{\tau_0}{\rho}}$$

$$u = \frac{\sqrt{\frac{\tau_0}{\rho}}}{\kappa} [\ln z - \ln z_0]$$

$$u = \frac{v_f}{\kappa} \ln \frac{z}{z_0}$$

where z_0 (m) is dependent on flow regimes governed by the shear Reynolds number,

$$R_* = \frac{v_f k_s}{\nu} ,$$

but is a non physical parameter. That is, physically, the velocity will not reach zero at a height of z_0 , and this is purely a consequence of the mathematical solution. The expressions for z_0 for different flow regimes are (Nielsen 2012),

- $z_0(R_* \leq 3) = \frac{0.11\nu}{v_f}$ - smooth laminar flow.
- $z_0(3 \leq R_* \leq 70) = \frac{0.11\nu}{v_f} + \frac{k_s}{30}$ - Transitional flow.
- $z_0(R_* \geq 70) = \frac{k_s}{30}$ - Fully rough turbulent flow.

For functional purposes, the z_0 value for the log law is usually represented as $z_0 = \frac{k_s}{30} + \frac{0.11\nu}{v_f}$,

where the first term dominates in turbulent flow, and the second term dominates in laminar flow (Nielsen 2012).

Data collected by Nikuradse (1950) demonstrated the change in velocity distribution with respect to hydraulic roughness. The results have shown the log law velocity distribution to be correlated well for fully rough flow and smooth laminar flow, but poorly correlated for the transitional zone (Callaghan 2014b). Adjustments were made such that the parameter z_0 was as follows:

$$z_0 = k_s e^{-\kappa\{\dots\text{curve_fit}\dots\}}, \quad (4.16)$$

where the curve fit parameter is empirical. The full semi empirical equation can be given as:

$$z_0 = k_s e^{-\kappa\left\{\frac{\frac{1}{\kappa} \ln \frac{k_s}{0.11\nu/v_f} + \frac{0.0065(\frac{k_s}{\nu/v_f})^{2.84}}{0.0022(\frac{k_s}{\nu/v_f})^{2.5} + 1} + \frac{767 \cdot 10^{-6}(\frac{k_s}{\nu/v_f})^{2.84} + 1}{767 \cdot 10^{-6}(\frac{k_s}{\nu/v_f})^{2.84} + 1}}\right\}} \quad (\text{Callaghan 2014a}). \quad (4.17)$$

The log law velocity distribution in this form has shown to 'collapse' onto the data with excellent correlation, as shown in Appendix 7.

However, research has also shown elements in the log law are subject to change dependent on its application. Non universality of Von Karmen's constant has been demonstrated by a number of studies, indicating the irregularity of the surface roughness and the relative submergence level induce the formation and evolution of turbulent structures. Recommended Von Karmen constants can range from 0.2 to 0.45, (Cooper 2006; Koll 2006; Manes et al. 2006; Nikora et al. 2001).

Ashida and Bayazit (1973) found that once $\frac{d}{k_s} < 3.3$, flow resistance is higher than what can be predicted by the log law (equation (4.3)), due to the form drag contributions in addition to the skin friction considered for small scale roughness. Large scale roughness induces wake and separation zones behind each roughness element, causing the generation, spreading and dissipation of turbulent vortices which are typically difficult to quantify with an equation. In conjunction with recommendations given by James (2002), a better way to model flow resistance may be through equations capable of explicitly modelling form drag, such as equation (4.15).

It is important to note the presence of secondary flows and drag at intermediate and large roughness scales may affect the z_0 component of the log law, although it is expected this will be a better approximation of velocity distribution than the Manning equation due to its physical basis. The following section outlines a comparison of the two methods.

4.6 Comparison of Methods

There are a plethora of ways to model hydraulic resistance in hydrodynamic flow at shallow depths. The most physical, most meaningful method of comparison is to plot experimental data on graph of $\frac{\bar{V}}{u_f}$ versus \mathbb{R} or $\frac{d}{k_s}$. This will give a relationship between hydrodynamic shear,

uniform velocity and flow regime or relative submergence. It is hypothesized this methodology will highlight the issue of the Manning's formula being only applicable for uniform flow and will give the limits of its use based on roughness scale and/or flow regime.

The most universally applicable method of modelling hydraulic resistance will be determined from this analysis and will be implemented into the TUFLOW source code.

4.6.1 Procedure

A variety of data for shallow flow was collected by Jordanova (2008), where normal depth was measured using a downstream V-notch weir from a known inflow. Roughness height and roughness element pattern were varied. A summary of the experiment type can be found in Appendix 8. The data was lumped into 4 categories, which pertained to the layout of roughness elements and their sizes. Parallel elements were labelled "Parallel", and ones which weren't parallel were labelled "Staggered". Roughness elements not varying in size were labelled "uniform", and ones varying in size were labelled "non-uniform". The friction velocity was calculated as $U_f = \sqrt{Sgd}$. The roughness height was calculated using methods outlined by Allen et al. (2007) using a calculator created in matlab, in which a sample calculation and calculator can be found in Appendix 5. A breakdown of the data can be found in Appendix 8.

4.6.2 Results

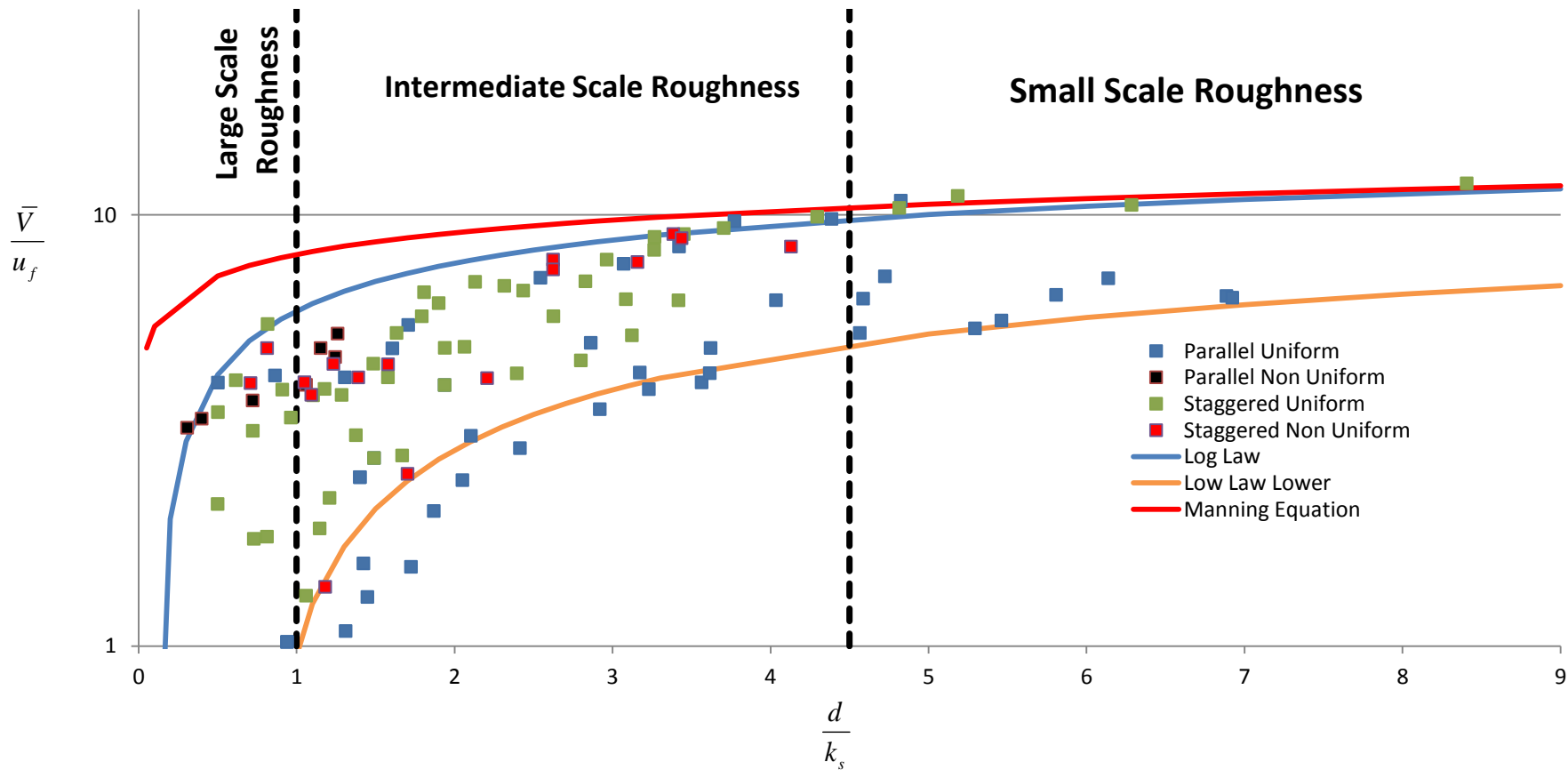


Figure 16 - Comparison of the Law of the Wall and the Manning Equation with the relationship between normalised velocity and relative roughness; showing all three relative roughness regions. Data was sourced from Jordanova (2008).

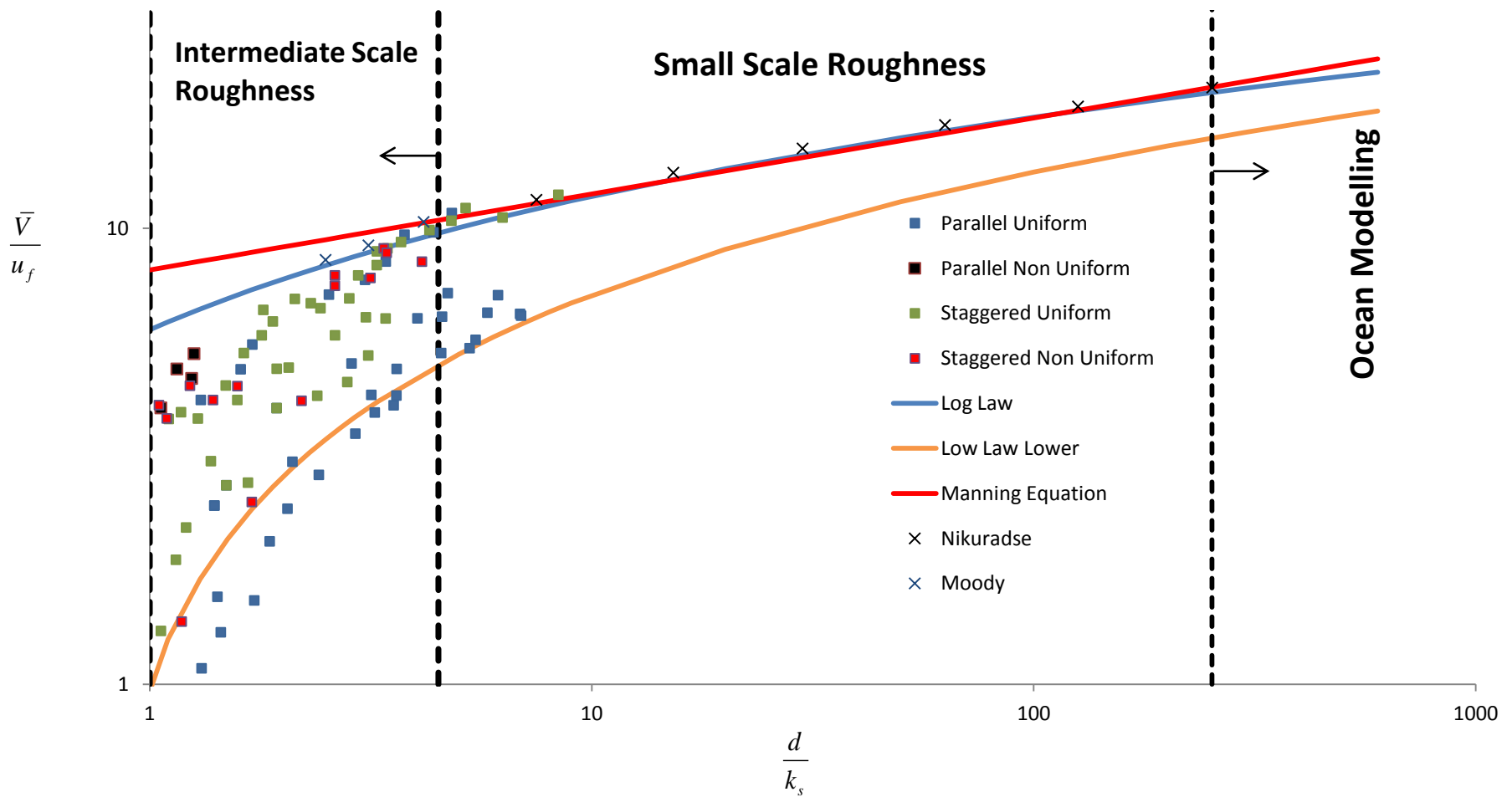


Figure 17 - Recreated velocity distribution over intermediate scale roughness, small scale roughness, and relative submergences which aren't suitable to model using a bed shear formula (i.e. ocean modelling). Data is graphed with normalised mean velocity on the Y axis, and relative submergence on the X axis. 'Nikuradse' and 'Moody' data was received from the original reports (Nikuradse 1950)

As evident in Figure 16, Non-uniformity in both the roughness size and element configuration create a large amount of variance in comparison to the data collected by Nikuradse (1950), which was matched remarkably well by *The Log Law* curve in Figure 17. From Figure 16 it is evident pattern effects have little influence on the variance of the normalised velocity, however uniformity effects seem to play an extremely significant role. Methods outlined by Allen et al. (2007) to account for non-uniformity in the roughness helped the data to 'collapse' into a more logical range of normalised velocity - however, this was not effective enough to 'collapse' the data onto one curve. This demonstrates the prevalence of secondary flows and drag forces which are not accounted for by the *Law of the Wall*. It is important to note that the adjustment of this data and graphing on different axes with the inclusion of factors such as z_0 , \mathbb{R} , and \mathbb{R}_* will simply shift the mean of the data, but scatter will still be significant. The scatter experienced is solely a consequence of the non-uniformity of bed roughness.

These issues arise partly due to the fact the log law requires uniform roughness (which Nikuradse was able to achieve in his experiments), but also because it was originally derived for bed shear only, not the total shear in the fluid. The conceptual layout for dimensional analysis of the log law is set out as follows;

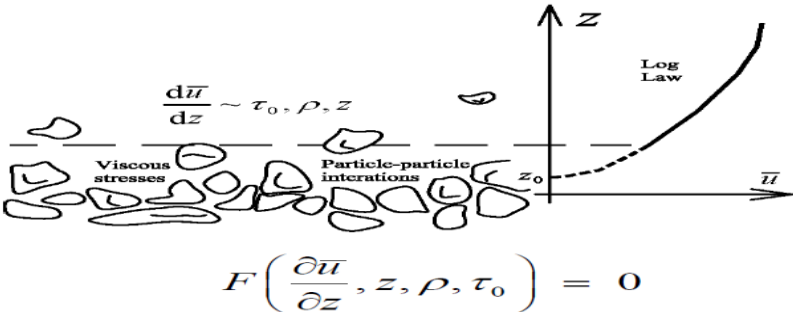


Figure 18 - Conceptual layout of the Law of the Wall for dimensional analysis. Mean velocity changes over the depth of the fluid and is dependent on bed shear, fluid density, and height within the fluid.

Rather than using τ_0 as a relevant variable of use in the π group, τ should be used - requiring the need for variables d and z_0 . Dimensional analysis leads to the following relationship;

$$\frac{\frac{\partial u}{\partial z} z}{\sqrt{\frac{\tau_0(1-\frac{z}{d})}{\rho}}} = \phi\left(\frac{d}{z_0}\right) \quad (4.18)$$

Because this cannot be solved, the simplified method must be used (using τ_0 instead of τ in analysis). This accounts for some discrepancy between the predictions and actual data. Although it is apparent differences exist, it is important to know what bearing this will have on the accuracy of the Shallow Water Equations.

As apparent in Figure 16, these differences will have some significant effect on the output of the hydraulic model; as the prevalence of secondary flows cause variance in flow velocity which can't be accurately estimated by any variation of *Log Law* or Manning equation in Figure 17. The depth of these conclusions are also limited by the fact that this analysis is based purely on a single data set, such that only rudimentary analyses have been performed.

Due to this reason, the practical implications for a real life catchment must be fully understood. The procedure and theory behind this can be found in Section 4.8.

4.7 Law of the Wall Implementation Into Numerical Model

Given the more appropriate fit to the data in comparison to other methods considered, the *Law of the Wall* will be implemented into TUFLOW Classic to determine its effectiveness in *direct rainfall modelling* on large rural and urban catchments. The source code for this hydrodynamic modelling software is written in FORTRAN, whose name is derived from FORMula TRANSlation. This computer language can be utilised to trigger a series of operations using binary patterns called operation codes, in order to execute a program. This basis is used to implement the shallow water equations at high computational efficiency and will need to be adapted to replace Manning's equation with the log law.

The fully implicit nature of the TUFLOW Classic framework necessitates the use of matrices to solve for the output, and given the complexities of creating a user interface using GIS and text editors; it is more effective to replace Manning's n with the log law parameters considering it is a temporary alteration. It can be illustrated as follows;

Manning Equation: $\bar{v} = \frac{1}{n} S^{1/2} R_h^{2/3}$

Law of the Wall: $\bar{v} = \frac{V_f}{\kappa} \ln \frac{d}{z_0 e}$

$$R_h = d$$

$$\frac{1}{n} S^{1/2} d^{2/3} = \frac{\sqrt{S g d}}{\kappa} \ln \frac{d}{z_0 e}$$

Rearrange for n: $n = \frac{d^{1/6} \kappa}{\sqrt{g}} \cdot \frac{1}{\ln \frac{d}{z_0 e}}$

$$z_0 = \frac{0.11 \nu}{v_f} + \frac{k_s}{30}$$

The relevant part of the source code is available for viewing in Appendix 9.

Dependent on the success of the method in a *direct rainfall model* in a practical situation, it may be permanently implemented into the TUFLOW framework.

4.8 Practical Implications of Secondary Flows

4.8.1 Introduction

As discussed in Section 4.6.2, secondary flows are evident from the presence of non-uniformity in the bed roughness. Considering the diversity of overland flow surfaces in real life applications, it is highly unlikely the surface roughness conditions will ever be fully uniform. For these reasons, it is important to determine the effect these secondary flows have on the design flow rate of a given sub-catchment.

By producing a set of independent and identically distributed numbers, relationships can be drawn from the non-uniformity in bed roughness and the induced effects of secondary flows on the model output. A Monte Carlo Type 1 simulation is an appropriate method to achieve this methodology, where a set of pseudo-random numbers are computed in which each number x_n is independent and identically distributed to x_{n-1} and x_{n+2} (Sauer 2012). This simulation can be utilised on roughness elements within a given catchment to determine these relationships.

For an urban catchment, the roughness of the roads and rooftops are well known due to the extensive research on these materials, especially work presented by Chow (1959). However, the unknown roughness components include things such as residential backyards due to the unknown landscape (e.g. grass length, presence of trees, garden ornaments etc.). Roughness components such as this contribute the majority of uncertainty in roughness estimation, and cause the majority of non-uniformity in bed roughness over the catchment.

It is hypothesised small catchments will be more sensitive to non-uniform bed roughness because the magnitude of the flow rate output is small in comparison to the magnitude of secondary flows produced. These effects have a lesser impact on the output as the catchment increases in size. Hence, the implications of secondary flows must be quantified with consideration given to the catchment size, and catchment land use.

4.8.2 Procedure

In order to utilise the Monte Carlo method, a hydraulic model was constructed for a small catchment in Bankstown, New South Wales. The catchment was 1 km² in size with average gradients of 3%. The land use of the catchment can be estimated as approximately 77% urbanised and 23% parks and recreational areas. A birds eye visual is supplied in Figure 19. The "PO" lines are plot output lines which measure the total flow across the distance of the line with respect to time.

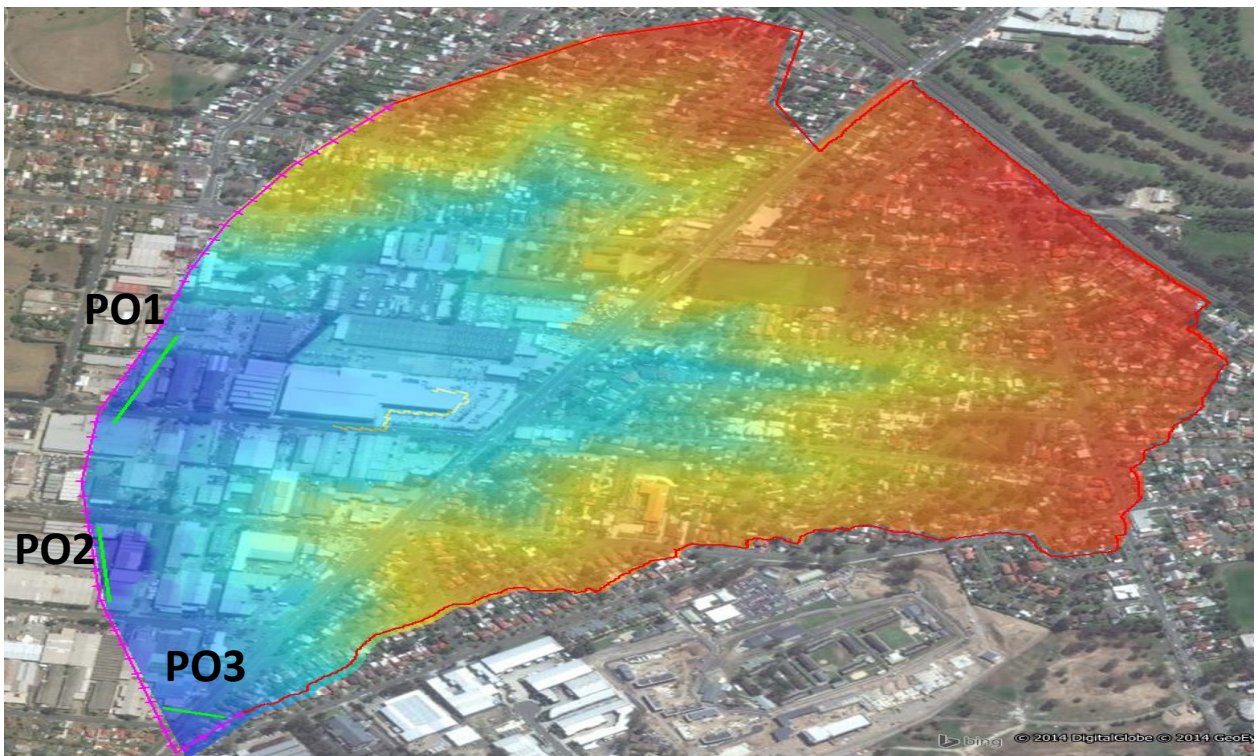


Figure 19 - Bankstown catchment aerial showing relative land use and catchment boundary. The “PO” lines correspond to data collection points at which the flow rate is recorded with time. High elevation is recorded in red in the Digital elevation map and low elevation in blue.

In order to simulate the unknown backyard roughness, a cadastre property boundary was retrieved and the GIS package was used to cut out the road and building content from each property, in order to create a land use layer in which the roughness could be assigned a random number.

A Matlab script (found in Appendix 10) was utilised to generate Manning's n coefficients between 0.02 and 0.15, to which each of the 685 cadastral parcels were assigned an individual roughness. 100 iterations were produced and run in the hydraulic model to produce 68,500 permutations of land use roughness. A *direct rainfall model* was used to apply a storm of 10% AEP over the catchment and the plot output lines were analysed using Microsoft VBA and Matlab (in which **all** statistics shown below were calculated)(found in Appendix 10).

4.8.3 Results and Discussion

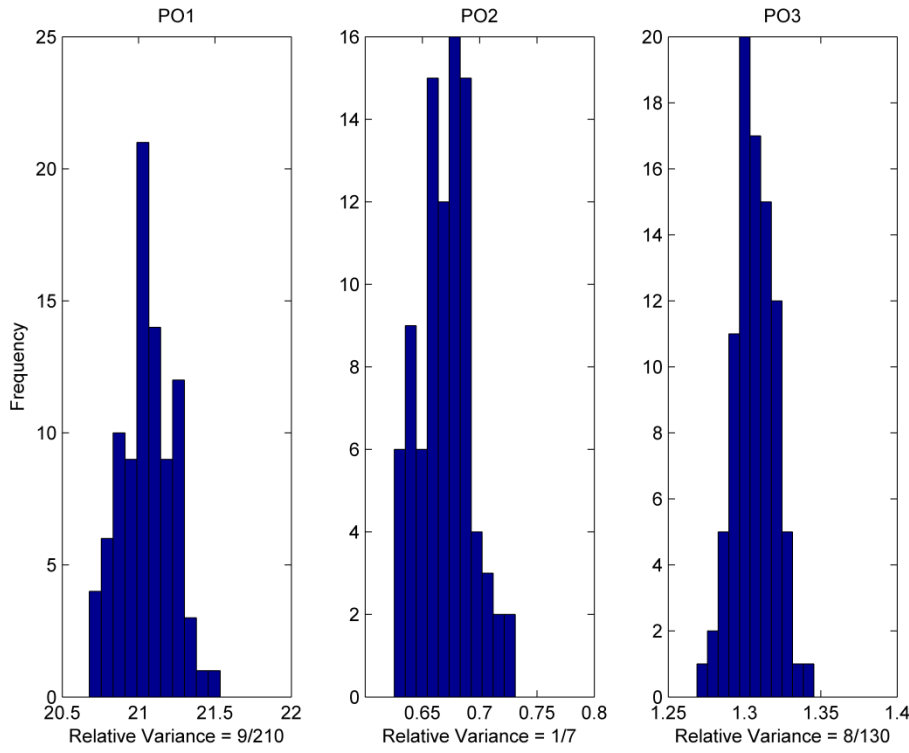


Figure 20 - Histograms of 'Plot Output' flow rates calculated with respect to variance in urban roughness. Frequency is shown on the vertical axis, and the relative variance in flow rate (m^3/s) is shown on the horizontal axis, which was calculated as a ratio of the flow range over the mean flow.

95% Confidence Intervals for flow rate (m^3/s) at each PO line

PO1	[20.7,21.3]
PO2	[0.6,0.7]
PO3	[1.3, 1.3]

Table 5 - 95% confidence intervals for flow rate at each of the plot output lines shown in Figure 19.

As evident in Figure 20, the variance in flow rate as a result of the non-uniformity in bed roughness appears to be normally distributed, with the only slight instance of any skewness or kurtosis occurring at *PO2*. Proof of this can be found in the Matlab output in Appendix 10. Relative variance is shown to decrease as the mean flow rate increases for each PO line, meaning the variance caused by secondary flows is less relevant as the catchment increases in size. This is

shown through the small relative variance in *PO1*, which significantly increases by an order of magnitude for *PO2*.

The confidence intervals in Table 5 show that in terms of practicality, the allowable variance from non uniformity in bed roughness depends on the desired goals of the modeller. For instance, in the context of a hydrologic model, the relative variance is extremely small hence insignificant in the overall scheme, so non-uniformity of roughness is not important. However, if the model is designed to determine what occurs at a micro scale (such as street and house inundation), the secondary flows cause variance in predictions which would be unsuitable to accept.

A useful caveat for the flood modeller is to note the output is normally distributed. This result allows a reasonable assumption of using the 3-sigma rule to calculate a 95% confidence interval, which is useful in practical situations where the modeller is interested in what kind of variance their model will experience, without the need to run it one hundred times. The modeller can be approximately 95% confident the flow will lie between the approximate bounds shown as follows, after only running the model a few times;

$$CI(95\%) = (\mu - 2\sigma, \mu + 2\sigma) \quad (4.19)$$

Where μ is the mean outputted flow rate, and σ is the standard deviation of the outputted flow rate.

In summary, the variance due to the presence of secondary flows onset from non-uniform bed roughness is only significant if a fine level of detail is required within the model. Considering this, no numerical model will ever produce a real life event with 100% accuracy. Given the very small size of the catchment and the amount of uncertainty present in the method of defining urban roughness, these results present a negligible amount of variance in the flow rate outputs - concluding non-uniformity in bed roughness has very little effect on output in even the smallest catchments.

5 Conclusion and Further Research Directions

The purpose of this industry thesis was to determine how to model shallow flow in the context of a *direct rainfall model*, with the feasibility of using *direct rainfall models* as hydrologic models as the overarching theme. The two dimensional shallow water model, TUFLOW GPU, was validated using Dressler's analytical solution in a sloped dam break situation to determine its accuracy. A comparison was undertaken between a *direct rainfall model* and an industry standard hydrologic model by their ability to reproduce the hydrology of a real life event in a gauged catchment. Hydraulic resistance mechanisms in shallow flow situations were explored and their applicability at different roughness scales were quantified. Literature was explored to determine feasible methods of modelling shallow flow, and a suitable method was implemented into TUFLOW following data analysis at shallow flow. The practicality of the method was assessed in a real catchment.

Research has progressed as far as necessary in terms of the model validation methodology and results analysis. Considering Dressler's downhill dam break analytical solution is the most difficult validation option available for numerical shallow water models to reproduce, no further research is required to find another validation test. The shape and magnitude of the depth versus time curves produced from TUFLOW GPU matched Dressler's solution with high accuracy, indicating both dry fronts were captured correctly and the model has no issues with the mathematics behind the Dressler's downhill dam break analytical solution. The model is deemed fit for purpose as a hydraulic model in this study and no further analysis is required.

Using some well established hydrology software, XP RAFTS, a comparison was undertaken on a gauged catchment in Durrumbul using TUFLOW GPU's direct rainfall features. In terms of reproducing the hydrology for a 2012 January storm event, TUFLOW GPU matched the shape of the stream gauge hydrograph in the Durrumbul catchment with more accuracy when compared to XP RAFTS. It was concluded the abrupt topography changes and poorly defined flow paths meant the nonlinear reservoir equation routing method was too simplified, whereas the GIS features in TUFLOW GPU and the use of the shallow water equations meant a high level of accuracy was captured. The TUFLOW GPU model was found to have a computation time approximately an order of magnitude slower than the hydrologic model, although both software

took a similar time to set each of the models up. However, the catchment was unsophisticated and reasonably homogeneous in terms of land use (and was not urbanised), such that a fairly low level analysis was performed. It is recommended more research be done into the sophistication (size and drainage features etc.) of different types of catchments and how it may affect hydrologic and hydraulic models.

Mechanisms regarding hydraulic resistance were determined to be related to the flow regime, which was dependent on the relative submergence, $\frac{d}{k_s}$. Large scale roughness conditions ($\frac{d}{k_s} < 1$) must contain the correct synergy of bed shear, element drag force, and secondary flows in order to be modelled correctly - whereas small scale roughness conditions ($\frac{d}{k_s} > 5.5$) need only consider bed shear to be modelled correctly.

The literature explored to determine suitable shallow flow modelling methods suggested empirical equations, variations of the Manning equation, and logarithmic equations to be applicable. The refined scope of the thesis limited the depth of conclusions able to be drawn, given only rudimentary analyses were performed. After analysis of a single set of data for shallow flow in an open channel, it was determined the *Law of the Wall* aka *The Log Law* is more suitable than Manning equation for modelling shallow flow. Secondary flows induced by the presence of non-uniformity in bed roughness created significant scatter in the data. It was concluded the 'Law of the Wall' was a better fit, but further research is required into the mechanisms of secondary flow, such as the presence of roll waves under large scale roughness conditions. The presence of drag forces and form losses in large scale roughness also proved too significant to be modelled accurately by the *Law of the Wall*. This was largely due to the fact this method was derived assuming bed shear as the dominant resistant force. As a result, it is recommended further studies be conducted for emergent flows (large scale roughness) to develop a suitable modelling method. It is highly recommended a comprehensive study on drag coefficients is conducted. Overall, the limited depth of the conclusions drawn warrant the need for more data for shallow flow in open channels. The next step in this research would be to verify these conclusions align with other experimental shallow flow data.

The practical implications of secondary flows were explored on a practical level by utilising Monte Carlo methods to analyse the outputted flow rates on a real urban catchment in Bankstown. On an extremely small catchment (1 km²), one hundred models were created and ran with variance in the roughness of cadastral parcels to simulate non-uniform bed roughness. It was concluded the variance in flow rate as a result of non-uniformity in bed roughness was negligible for hydrologic uses of the model, but significant if an intricate study was being investigated, such as quantifying insurance claims for house inundation on an urban catchment. Due to the rudimentary level of analysis undertaken, it is recommended similar studies are conducted exploring more intricate areas in finer detail.

6 References

Adams, A 1991, 'Application and comparison of RORB, WBNM and RAFTS runoff routing models', in *International Hydrology and Water Resources Symposium 1991 Part 2 (of 3), October 2, 1991 - October 4, 1991*, Perth, Aust, vol. 2, pp. 485-91.

Allen, JJ, Shockling, MA, Kunkel, GJ & Smits, AJ 2007, 'Turbulent flow in smooth and rough pipes', *Philos Trans A Math Phys Eng Sci*, vol. 365, no. 1852, pp. 699-714.

Anonymous 2007, *Sobek Advanced Version 2.10.003 - User Manual*, The Netherlands.

— 2009, *OpenCL Programming Guide for the CUDA Architecture*, viewed 3/15/2014, <http://www.nvidia.com/content/cudazone/download/OpenCL/NVIDIA_OpenCL_ProgrammingGuide.pdf>.

— 2013, 'Matlab - 2013b'.

— 2014, 'MapInfo Professional'.

Ashida, K & Bayazit, M 1973, 'Initiation of motion and roughness of flows in steep channels', *Proceedings - International Association for Hydraulic Research Congress = Congres de l'Association Internationale de Recherches Hydrauliques*, no. 15, Vol.1, pp. 475-84.

Bathurst, JC, Li, RM & Simons, DB 1981, 'Resistance equation for large-scale roughness', *Journal of the Hydraulics Division, ASCE*, vol. 107, no. HY12, Proc. Paper 16743, pp. 1593-613.

Borah, DK 2011, 'Hydrologic procedures of storm event watershed models: A comprehensive review and comparison', *Hydrological Processes*, vol. 25, no. 22, pp. 3472-89.

Bray, DI & Davar, KS 1987, 'Resistance to flow in gravel-bed rivers', *Canadian Journal of Civil Engineering*, vol. 14, no. 1, pp. 77-86.

Caddis, B, Jempson, M, Ball, JE & Syme, W 2008, 'Incorporating Hydrology into 2D Hydraulic Models - the Direct Rainfall Approach', paper presented to National Conference on Hydraulics in Water Engineering (9th: 2008: Darwin, NT), Barton, A.C.T., 2008, <<http://search.informit.com.au/documentSummary;dn=613534512422906;res=IELENG>>.

Callaghan, DP 2014a, 'Log Law Velocity Distribution - Modified Equation'.

— 2014b, 'A.XXX.V03Work1_Lowlaw_Update Lecture Notes'.

Callaghan, DP, Ahmadi, A & Nielsen, P 2011, 'Transient wave behaviour over an underwater sliding hump from experiments and analytical and numerical modelling', *Experiments in Fluids*, vol. 51, no. 6, pp. 1657-71.

Carroll, DG 1998, 'URBS - A Catchment Management & Flood Forecasting Rainfall Runoff Routing Model', pp. 5-35.

Chanson, H 2014, *Applied hydrodynamics: an introduction*, CRC Press, Taylor & Francis Group, Boca Raton.

Chippada, S, Dawson, CN, Martinez, ML & Wheeler, MF 1998, 'A Godunov-type finite volume method for the system of shallow water equations', *Computer Methods in Applied Mechanics and Engineering*, vol. 151, no. 1-2, pp. 105-29.

Chow, VT 1959, *Open-Channel Hydraulics*, ed. McGraw-Hill, New York.

Clark, KMB, J.E. Babister, M.K. 2008, 'Can Fixed Grid 2D Hydraulic Models be Used as Hydrological Models?', in MD Lambert, TM; Leonard, Michael (ed.), *Proceedings of Water Down Under 2008*, Modbury, SA.

Collecut, G 2014, *TUFLOW GPU Release Notes*.

Cooper, JR 2006, *Spatially-induced Momentum Transfer Over Water-worked Gravel Beds*, University of Sheffield, Department of Civil and Structural Engineering.

Crowe, CT 2009, *Engineering fluid mechanics*, John Wiley & Sons, Hoboken, NJ.

Cunge, JAH, F.M., Jr; Verwey, A. 1980, *Practical aspects of computational river hydraulics*, Pitman Adv. Publ. Prog., Boston, MA, United States.

Dingman, SL & Sharma, KP 1997, 'Statistical development and validation of discharge equations for natural channels', *Journal of Hydrology*, vol. 199, no. 1-2, pp. 13-35.

Downer, CW & Ogden, FL 2004, 'GSSHA: Model to simulate diverse stream flow producing processes', *Journal of Hydrologic Engineering*, vol. 9, no. 3, pp. 161-74.

Dressler, RF 1958, 'Unsteady Non-Linear Waves in Sloping Channels', *Proceedings of the Royal Society of London. Series A, Mathematical and Physical Sciences*, vol. 247, no. 1249, pp. 186-98.

Garcia Diaz, R 2005, 'Analysis of Manning coefficient for small-depth flows on vegetated beds', *Hydrological Processes*, vol. 19, no. 16, pp. 3221-33.

- Gimenez, R & Govers, G 2001, 'Interaction between bed roughness and flow hydraulics in eroding rills', *Water Resources Research*, vol. 37, no. 3, pp. 791-9.
- Hall, J 2014, 'Direct Rainfall Modelling: The good, the bad and the ugly', paper presented to Hydrology & Water Resources Symposium 2014, Perth.
- Hessel, R, Jetten, V & Zhang, G 2003, 'Estimating Manning's n for steep slopes', *Catena (Giessen)*, vol. 54, no. 1-2, pp. 77-91.
- James, CB, A.; Jordanova, A.; Kotschy, K.; Nicolson, C.; Makoa, M.; 2002, 'Interaction of Reeds, Hydraulics and River Morphology', in Water Research Commission, South Africa.
- Jarvela, J & Aberle, J 2007, 'Comment on 'Analysis of Manning coefficient for small-depth flows on vegetated beds' by R. Garcia Diaz', *Hydrological Processes*, vol. 21, no. 16, pp. 2206-8.
- Jordanova, A 2008, 'Low Flow Hydraulics in Rivers For Environmental Applications in South Africa'.
- Kalyanapu, AJ, Shankar, S, Pardyjak, ER, Judi, DR & Burian, SJ 2011, 'Assessment of GPU computational enhancement to a 2D flood model', *Environmental Modelling & Software*, vol. 26, no. 8, pp. 1009-16.
- Kibler, DFR, Joseph R 1991, 'Runoff Resistance of a Textured Surface Under Simulated Rainfall'.
- Koll, K 2006, 'Parameterisation of the vertical velocity profile in the wall region over rough surfaces', in *River Flow 2006, Two Volume Set*, Taylor & Francis, viewed 2014/09/17, DOI doi:10.1201/9781439833865.ch15
10.1201/9781439833865.ch15, <<http://dx.doi.org/10.1201/9781439833865.ch15>>.
- Koren, V, Reed, S, Smith, M & Zhang, Z 2003, 'Combining physically-based and conceptual approaches in the development and parameterization of a distributed system', *IAHS-AISH Publication*, no. 282, pp. 101-8.
- Kuczera, G 1999, 'Comprehensive at-site flood frequency analysis using Monte Carlo Bayesian inference', *Water Resources Research*, vol. 35, no. 5, p. 1551.
- Kuo, F-A, Smith, MR, Hsieh, C-W, Chou, C-Y & Wu, J-S 2011, 'GPU acceleration for general conservation equations and its application to several engineering problems', *Computers and Fluids*, vol. 45, no. 1, pp. 147-54.
- LeVeque, RJ 2002, *Finite volume methods for hyperbolic problems*, Cambridge University Press, New York; Cambridge.

Liu, CL & Chen, YQ 2008, 'Application of geographic information system in hydrological models', in *From Headwaters to the Ocean*, CRC Press, pp. 217-22, viewed 2014/03/15, DOI doi:10.1201/9780203882849.ch32

10.1201/9780203882849.ch32, <<http://dx.doi.org/10.1201/9780203882849.ch32>>.

Maheshwari, BL 1992, 'Suitability of different flow equations and hydraulic resistance parameters for flows in surface irrigation: a review', *Water Resources Research*, vol. 28, no. 8, pp. 2059-66.

Manes, C, Pokrajac, D, McEwan, I, Finnigan, JJ & Nikora, V 2006, 'On the definition of the shear velocity in rough bed open channel flows', in *River Flow 2006, Two Volume Set*, Taylor & Francis, viewed 2014/09/17, DOI doi:10.1201/9781439833865.ch7

10.1201/9781439833865.ch7, <<http://dx.doi.org/10.1201/9781439833865.ch7>>.

Muncaster, SB, W. McCowan, A. 2006, 'Design Flood Estimation in Small Catchments using Two-dimensional hydraulic modelling - a case study', in *30th Hydrology and Water Resources Symposium*, Launceston, TAS.

Nielsen, P 2012, '*Uniform Flows*, Lecture notes distributed in Fluid Mechanics for Civil and Environmental Engineers at The University of Queensland, on 12 September 2012.'

Nikora, V, Goring, D, McEwan, I & Griffiths, G 2001, 'Spatially Averaged Open-Channel Flow over Rough Bed', *Journal of Hydraulic Engineering*, vol. 127, no. 2, pp. 123-33.

Nikuradse, J 1950, *Laws of flow in rough pipes*, National Advisory Committee for Aeronautics Washington.

Popovich, A & Hummel, R 1967, 'Experimental study of the viscous sublayer in turbulent pipe flow', *AIChE Journal*, vol. 13, no. 5, pp. 854-60.

Raudkivi, AJ 1963, 'Estimation of roughness coefficient from velocity measurements in open channels', *J. Hydrol*, vol. 2, pp. 53-6.

Rehman, H 2011, *Rainfall-on-Grid Modelling - a Decade of Practice*.

Rehman, H, Zollinger, M & Collings, G 2003, *Hydrological vs Hydraulic Routing Possibilities with Two-dimensional Hydraulic Modelling*.

Sauer, T 2012, *Numerical analysis*, Pearson, Boston.

Schlichting, H, Gersten, K & Gersten, K 2000, *Boundary-layer theory*, Springer.

Sharpe, R & James, C 2007, 'Deposition of sediment from suspension in emergent vegetation', *Water SA*, vol. 32, no. 2, pp. 211-8.

Syme, W 2006, *TUFLOW User Manual*, ed. W Oceanics, Australia.

Toro, EF 2009a, 'The Riemann Solver of Roe', in Springer Berlin Heidelberg, Berlin, Heidelberg, pp. 345-76, DOI 10.1007/b79761_11,
<http://uq.summon.serialssolutions.com/2.0.0/link/0/eLvHCXMwY2BQSLQwM0tOTUo0B9YPLiYpqRZJwEarqUVqUhLouHKDVJSxDqTS3E2IqSk1T5TBzM01xNIDFzYxGV8AOXchHjGTb2JpYWYiaxYPL EzNzeJBK_WBWVaMgQXYY04FAKqcH4Q>.

—— 2009b, *Riemann Solvers and Numerical Methods for Fluid Dynamics: A Practical Introduction*, Springer Berlin Heidelberg, Dordrecht.

Turner, AK & Chanmeesri, N 1984, 'Shallow flow of water through non-submerged vegetation', *Agricultural Water Management*, vol. 8, no. 4, pp. 375-85.

Von Karman, T 1975, *Collected works of Theodore Von Karman, 1952-1963*, Von Karman Institute for Fluid Dynamics, Rhode-St-Genese, Belgium U6 - ctx_ver=Z39.88-2004&ctx_enc=info%3Aofi%2Fenc%3AUTF-8&rft_id=info:sid/summon.serialssolutions.com&rft_val_fmt=info:ofi/fmt:kev:mtx:book&rft.genre=book&rft.title=Collected+works+of+Theodore+Von+Karman%2C+1952-1963&rft.au=Von+Karman%2C+Theodore&rft.date=1975-01-01&rft.pub=Von+Karman+Institute+for+Fluid+Dynamics&rft.externalDBID=n%2Fa&rft.externalDocID=b14583392¶mdict=en-US U7 - Book U8 - FETCH-uq_catalog_b145833921.

Wood, EF, Sivapalan, M, Beven, K & Band, L 1988, 'Effects of spatial variability and scale with implications to hydrologic modeling', *Journal of Hydrology*, vol. 102, no. 1, pp. 29-47.

Yen, B 1992, 'Dimensionally Homogeneous Manning's Formula', *Journal of Hydraulic Engineering*, vol. 118, no. 9, pp. 1326-32.

—— 2002, 'Open channel flow resistance', *Journal of Hydraulic Engineering*, vol. 128, no. 1, pp. 20-39.

Appendix 1 - Dressler Dam Break

Refer to attached CD for Appendix 1.

Appendix 2 - Pearson Correlation for Dressler's Dam Break Solution

Dimensionless Position	Correlation (Pearson r)
-0.5	1.000
0.5	0.998
1	0.996
2	0.997

Table 6 - Lack of Fit Assessment of TUFLOW GPU to Dressler's Solution

As evident in Figure 5, the movement of the water mass down the slope is very intuitive and makes physical sense. Flow is unsteady given the boundary layer is not given enough space to develop, and as a result, variation in Manning's n does not alter the results significantly, albeit more variation in results is experienced with greater distance from the shock.

As previously mentioned, this benchmark test is the most difficult for a numerical model to match given the two dry fronts which is generally a numerical issue, and also matching the solution given the singularity experienced in the analytical solution - which is a mathematical issue. As apparent in Table 6, the TUFLOW GPU solution matches the analytical solution very nicely visually, but also correlates extremely well using a Pearson r correlation, which states

$$r = \frac{\sum (x - \bar{x})(y - \bar{y})}{\sqrt{\sum (x - \bar{x})^2 \sum (y - \bar{y})^2}} .$$

This correlation adds further value to Figure 5, which showed a good prediction based on engineering judgement.

Appendix 3 - Sensitivity Testing of TUFLOW GPU

Refer to attached CD for Appendix 3.

Appendix 4 - TUFLOW GPU versus RAFTS on Gauged Catchment

Refer to attached CD for Appendix 4.

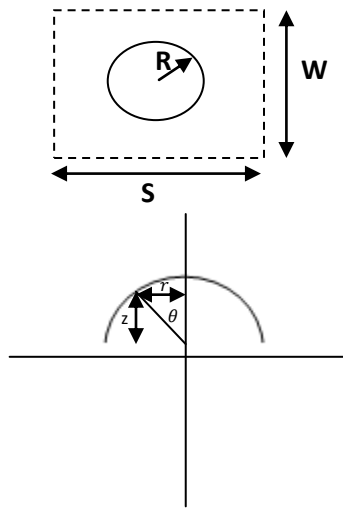
Appendix 5 - Roughness Calculation using the Root Mean Square of Surface Roughness

Refer to attached CD for the matlab roughness calculator for Appendix 5.

$$\bar{z} = \frac{\int z dA}{A}$$

$$z^2_{RMS} = \frac{\int (z - \bar{z})^2 dA}{A}$$

For an arbitrary area containing hemisphere of size R;



$$r = R \sin \vartheta$$

$$z = R \cos \vartheta$$

$$dA = 2\pi r dr$$

$$dr = R \cos \vartheta d\vartheta$$

$$\int z dA = \int_0^{\pi/2} R \cos \vartheta \cdot 2\pi R \sin \vartheta (-R \cos \vartheta) d\vartheta$$

$$\int z dA = \frac{2\pi}{3} R^3$$

For N elements of height R and r in a unit area;

$$A_s = \frac{1}{N}$$

$$\bar{z} = N_1 \frac{2\pi}{3} R^3 + N_2 \frac{2\pi}{3} r^3]$$

$$N_T = \sum_{i=1}^n N_i$$

$$z_{RMS} = \sqrt{\frac{(A_s - \pi R^2 - \pi r^2) \bar{z}^2 + \int_0^{\pi/2} R^2 \cdot 2\pi \cos \vartheta \sin \vartheta (R \cos \vartheta - \bar{z})^2 d\vartheta + \int_0^{\pi/2} r^2 \cdot 2\pi \cos \vartheta \sin \vartheta (r \cos \vartheta - \bar{z})^2 d\vartheta}{1 / N_T}}$$

where;

$$\int_0^{\pi/2} R^2 \cdot 2\pi \cos \vartheta \sin \vartheta (R \cos \vartheta - \bar{z})^2 d\vartheta = R^2 \left(\frac{\pi R^2}{2} - \frac{4}{3} R \bar{z} + \pi \bar{z}^2 \right)$$

Appendix 6 - TUFLOW Model for Large Scale Roughness Conditions (Emergent Reeds)

Refer to attached CD for Appendix 6.

Appendix 7 - Evidence of Data Collapse by Adjustment of z_0 parameter on the Log Law

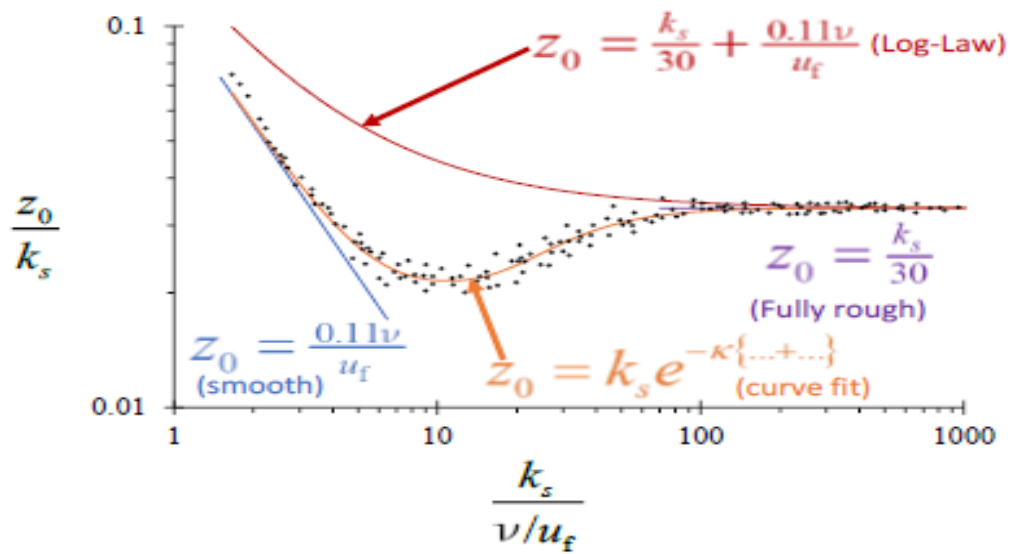


Figure 21 - Semi Empirical Log-Law evidencing better correlation in the transition zone by using a curve fit for z_0 .

Appendix 8 - Data Summary of Jordanova

Refer to attached CD for Appendix 8.

Appendix 9 - Source Code of the Log Law implementation into TUFLOW (in FORTRAN)

else if (MatTest(im).eq.MMT_Log) **then** ! True if material Manning's n based on 'The Law of the Wall' approach using a roughness height

```
    y = (h(i,j) + h(i,j+1))/2. - zu(i,j) ! Calculate depth at cell side (h water level and zu right side
    elevation)
    y = max(y, 0.00001) ! Ensure depth remains positive
    S = abs((max(h(i,j),zu(i,j)) - max(h(i,j+1),zu(i,j))))/dx ! Calculate water surface slope. Dry
    cell h = ground elevation.
    S = max(S, 0.00001) ! Ensure slope remains positive
    z0 = ks(im)/30. + 0.11*1.e-6/sqrt(S*g*y) ! Calculate Z0. im is material index. ks() roughness
    heights for each material. g = gravity.
    Mn(i,j) = Kk(im)*y**(1./6.)/(sqrt(g)*log(y/z0/2.71828)) ! Calculate equivalent Manning's n
    value for ks and depth. Kk() is Kappa.
```

Appendix 10 - Practical Implications of Secondary Flows

Refer to attached CD for Appendix 10.